Cellular/Molecular

mTORC2 Loss in Oligodendrocyte Progenitor Cells Results in Regional Hypomyelination in the Central Nervous System

Kristin D. Dahl,[1] Adam R. Almeida,[1] Hannah A. Hathaway,[1] Jennifer Bourne,[1†] Tanya L. Brown,[1] Lisbet T. Finseth,[1] Teresa L. Wood,[2] and Wendy B. Macklin[1]

[1]Department of Cell and Developmental Biology, University of Colorado School of Medicine, Aurora, Colorado 80045, and [2]Department of Pharmacology, Physiology and Neurosciences, Rutgers New Jersey Medical School, Newark, New Jersey 07103

In the CNS, oligodendrocyte progenitor cells (OPCs) differentiate into mature oligodendrocytes to generate myelin, an essential component for normal nervous system function. OPC differentiation is driven by signaling pathways, such as mTOR, which functions in two distinct complexes: mTOR complex 1 (mTORC1) and mTOR complex 2 (mTORC2), containing Raptor or Rictor, respectively. In the current studies, mTORC2 signaling was selectively deleted from OPCs in PDGFRα-Cre X Rictor^fl/fl mice. This study examined developmental myelination in male and female mice, comparing the impact of mTORC2 deletion in the corpus callosum and spinal cord. In both regions, Rictor loss in OPCs resulted in early reduction in myelin RNAs and proteins. However, these deficits rapidly recovered in spinal cord, where normal myelin was noted at P21 and P45. By contrast, the losses in corpus callosum resulted in severe hypomyelination and increased unmyelinated axons. The hypomyelination may result from decreased oligodendrocytes in the corpus callosum, which persisted in animals as old as postnatal day 350. The current studies focus on uniquely altered signaling pathways following mTORC2 loss in developing oligodendrocytes. A major mTORC2 substrate is phospho-Akt-S473, which was significantly reduced throughout development in both corpus callosum and spinal cord at all ages measured, yet this had little impact in spinal cord. Loss of mTORC2 signaling resulted in decreased expression of actin regulators, such as gelsolin in corpus callosum, but only minimal loss in spinal cord. The current study establishes a regionally specific role for mTORC2 signaling in OPCs, particularly in the corpus callosum.

Key words: actin; gelsolin; mTORC2; myelination; oligodendrocyte; Rictor

Significance Statement

mTORC1 and mTORC2 signaling has differential impact on myelination in the CNS. Numerous studies identify a role for mTORC1, but deletion of Rictor (mTORC2 signaling) in late-stage oligodendrocytes had little impact on myelination in the CNS. However, the current studies establish that deletion of mTORC2 signaling from oligodendrocyte progenitor cells results in reduced myelination of brain axons. These studies also establish a regional impact of mTORC2, with little change in spinal cord in these conditional Rictor deletion mice. Importantly, in both brain and spinal cord, mTORC2 downstream signaling targets were impacted by Rictor deletion. Yet, these signaling changes had little impact on myelination in spinal cord, while they resulted in long-term alterations in myelination in brain.

Introduction

Myelin is a specialized membrane generated by oligodendrocytes in the CNS, which allows saltatory conduction and provides trophic support to axons (Verden and Macklin, 2016). Differentiation of oligodendrocyte precursor cells (OPCs) into myelin-producing oligodendrocytes involves extreme metabolic and morphologic changes (Goldman, 1992), including altered myelin gene expression, lipid biosynthesis, and cytoskeleton organization, and these changes are driven by selective signaling pathways (Adams et al., 2021).

An important signaling pathway involved in oligodendrocyte differentiation is the mechanistic target of rapamycin (mTOR), a highly conserved serine/threonine kinase that regulates numerous

cellular processes (Saxton and Sabatini, 2017). mTOR functions in two distinct complexes: mTOR complex 1 (mTORC1), defined by the presence of Raptor; and mTOR complex 2 (mTORC2), defined by the presence of Rictor (Wood et al., 2013; Saxton and Sabatini, 2017). Numerous studies support an important role for mTOR signaling in OPC differentiation and myelination. Our early *in vivo* studies overexpressing constitutively active Akt in oligodendrocytes established that Akt signaling through mTOR drives oligodendrocyte differentiation and myelination, eventually resulting in hypermyelination (Flores et al., 2008; Narayanan et al., 2009). Pharmacological inhibition of mTOR *in vitro* blocks OPC differentiation (Tyler et al., 2009; Bercury et al., 2014), and siRNA knockdown of either Raptor or Rictor decreases myelin protein expression (Tyler et al., 2009). As OPCs differentiate, mTOR regulates myelin protein expression, lipid biosynthesis, and cytoskeletal actin dynamics (Bercury et al., 2014; Lebrun-Julien et al., 2014; Wahl et al., 2014; Mathews and Appel, 2016; Musah et al., 2020).

The two mTOR complexes have different substrates and functions, and the relative contribution of each complex to OPC differentiation and myelination is still poorly understood. Conditional deletion studies establish that mTORC1 (Raptor) or mTORC2 (Rictor) signaling impacts oligodendrocyte differentiation differently, depending on (1) the differentiation stage of oligodendrocytes and (2) the CNS region under investigation. Using the $2'$, $3'$ cyclic nucleotide $3'$-phosphodiesterase (CNP) promoter, which expresses Cre late in oligodendrocyte differentiation, mTOR or Raptor conditional deletion results in hypomyelination in spinal cord but not corpus callosum (Bercury et al., 2014; Lebrun-Julien et al., 2014; Wahl et al., 2014). Thus, mTORC1 signaling is required for myelination, although this requirement appears to be unique to specific regions of the CNS. By contrast, ablation of mTORC2 signaling in *CNP-Cre; Rictor*fl/fl mice has no impact on myelination in either spinal cord or corpus callosum (Bercury et al., 2014; Lebrun-Julien et al., 2014). Nevertheless, a role for mTORC2 was established by ablating Rictor throughout the oligodendrocyte lineage (i.e., from early developmental stages). Thus, in Olig2-Cre mice, Rictor conditional deletion results in delayed myelination in the corpus callosum (Grier et al., 2017). This suggests that mTORC2 signaling is necessary early in OPC differentiation but that loss of that signaling in CNP-Cre conditional deletion mice is not important or mTORC2 could be compensated for later in development. Grier et al. (2017) did not investigate whether mTORC2 signaling plays a similar role in other regions of the CNS, such as the spinal cord, nor did that study investigate the signaling pathways impacted by Rictor deletion.

Olig2-Cre expression in *Olig2-Cre; Rictor*fl/fl mice would result in mTORC2 deletion in precursor cells as early as embryonic day 9.5, preceding expression of platelet derived growth factor receptor α (PDGFRα) (Zhou et al., 2000). PDGFRα is expressed by OPCs in the CNS but is downregulated as oligodendrocytes differentiate, making PDGFRα a specific marker of the OPC stage of the oligodendrocyte lineage (Pringle et al., 1992; Pringle and Richardson, 1993). In the current study, we used PDGFRα-Cre mice to delete Rictor, and thereby mTORC2 signaling, selectively in OPCs, specifically impacting differentiation. This resulted in hypomyelination in corpus callosum, but interestingly the impact of Rictor deletion from OPCs was minimal in spinal cord. These data support unique developmental and region-specific requirements of mTOR signaling, and a particular role for mTORC2 signaling in OPC differentiation.

Materials and Methods

Mice models. Mice used in this study include PDGFRα-Cre mice (*C57BL/6-Tg(Pdgfra-cre)1Clc/*; JAX stock #013148; RRID:IMSR_JAX:013148) (Roesch et al., 2008) and Rictor^{fl/fl} mice (MMRRC B6.129S6(SJL)-Rictor[tm1.1Mgn]/Mmnc; RRID:MMRRC_014113-UNC) (Shiota et al., 2006). Heterozygous PDGFRα-Cre mice (Cre±) were bred with homozygous Rictor^{fl/fl} mice to obtain *PDGFRα-Cre±;Rictor*^{fl/+} mice. These mice were bred with Rictor^{fl/fl} mice to obtain Rictor conditional KO (cKO) mice (Rictor cKO; *PDGFRα-Cre±;Rictor*^{fl/fl}) and littermate control mice (*PDGFRα-Cre*^{+/+};Rictor^{fl/fl} or *PDGFRα-Cre*^{+/+};Rictor^{fl/+} mice). Both male and female mice were used in all analyses. Genotypes of all mice were determined by PCR using previously published primers and protocols, as well as primers defined by The Jackson Laboratory, oIMR1084 and oIMR1085 (Shiota et al., 2006; Roesch et al., 2008). The Rictor cKO animals (*PDGFRα-CRE±;Rictor*^{fl/fl}) had a significantly decreased body weight compared with control Cre-negative animals. Body weight analysis indicated the mean weight was 7.24 g (SEM 0.206; N = 22) for control mice and 5.899 g (SEM 0.194; N = 10) for Rictor cKO mice at P14, using an unpaired *t* test with Welch's correction $p = 0.000614$, df = 26.37. At P30, the mean was 16.48 g (SEM 0.692, N = 7) for control mice and 8.34 g (SEM 0.556, N = 11) for Rictor cKO mice, using an unpaired *t* test with Welch's correction $p = 0.0000005$; df = 13.00. For aged animals (ranging from P140 and P342), the mean was 34.24 g (SEM 2.006, N = 5) for control mice and 25.85 g (SEM 1.462, N = 4) for Rictor cKO mice, using an unpaired *t* test with Welch's correction $p = 0.0122$; df = 6.815. All animal procedures were conducted with the approval of the University of Colorado Institutional Animal Care and Use Committee.

To confirm that the cKO of Rictor was specific to PDGFRα-expressing OPCs, we used FACS to sort cells from control and Rictor cKO animals and performed RT-PCR from mRNA isolated from the sorted cells. Brain tissue was harvested from P7 control or Rictor cKO mice. Cells were dissociated using the Miltenyi Biotec Neural Dissociation Kit (order #130-092-628) per the manufacturer's specifications and sorted using the following antibodies: PDGFRα (BioLegend catalog #135905, RRID:AB_1953268) for OPCs, O4 (R&D Systems catalog #FAB1326P, RRID:AB_664169) for mature oligodendrocytes, CD45 (BioLegend catalog #157205, RRID:AB_2860725) for microglia, ASCA2 (Miltenyi Biotec catalog #130-123-284, RRID:AB_2811488) for astrocytes, and THY1.2 (BioLegend catalog #140331, RRID:AB_2894662) for neurons. RNA was isolated using the QIAGEN RNeasy Mini Kit (catalog #74104) per the manufacturer's specifications, and cDNA was synthesized using Bio-Rad iScript cDNA Synthesis Kit (catalog #1708890). The Rictor primer sequence was 5′-TCGATCTGACCCGAGAACCTT-3′ and 5′-GTTATTCAGATGGCCCAGCTTT-3′. The PCR was stopped at 30 cycles, which was determined to be within the PCR exponential phase. PCR products were run on a 2% agarose gel and imaged with a Bio-Rad gel imager. Rictor RNA expression in PDGFRα-positive cells from Rictor cKO mice was 11% of control, and Rictor RNA expression in O4-positive cells was 31% of control. By contrast, in CD45-positive cells, Rictor RNA expression was 102% of control; in ASCA-positive cells, expression was 175% of control; and in THY1.2-positive cells, expression was 86% of control.

Electron microscopy. Animals were perfused with modified Karnovsky's fixative (2% Paraformaldehyde [PFA]/2.5% glutaraldehyde) in phosphate buffer (PB), pH 7.4. The brain was removed and immersed in the same fixative overnight. Corpus callosum was isolated from 1 mm coronal slices of brain between −0.94 and −2.18 of bregma (Franklin and Paxinos, 2008). Spinal cords were cut into 500 nm coronal sections through the cervical enlargement. Using a PELCO Biowave Pro tissue processor (Ted Pella), the tissue was rinsed in 100 mM cacodylate buffer and then postfixed in a reduced osmium mixture consisting of 1% osmium tetroxide and 1.5% potassium ferrocyanide followed by 1% osmium tetroxide alone. Dehydration was conducted in a graded series of acetone (50%, 70%, 90%, 100%) containing 2% uranyl acetate for *en bloc* staining. Finally, tissue was infiltrated and embedded in Embed 812 (Electron Microscopy Services) and cured for 48 h at 60°C in an oven. The corpus callosum pieces were oriented such that sections could be cut midline in a sagittal plane. Spinal cord pieces were oriented such that sections could be cut in a transverse plane. Ultrathin
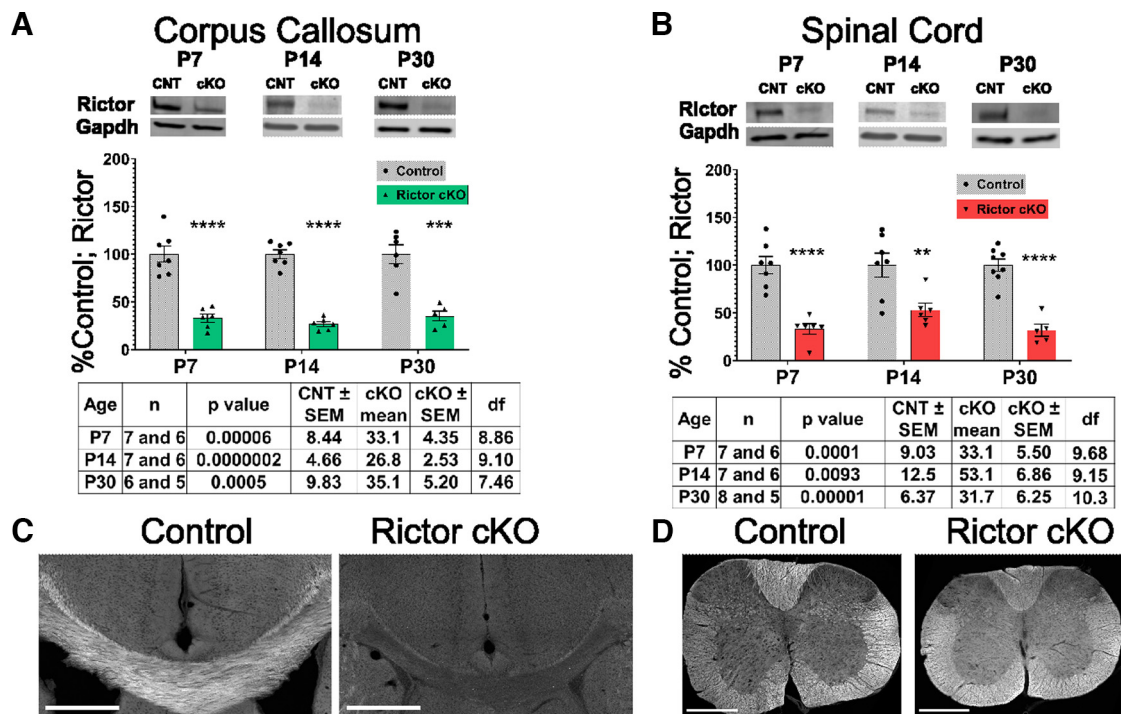
Figure 1. Rictor cKO in OPCs resulted in hypomyelination in the corpus callosum and not in the spinal cord. *A*, Rictor protein expression in corpus callosum normalized to GAPDH in Rictor cKO compared with control (CNT) at P7, P14, and P30. *B*, Rictor protein expression in spinal cord normalized to GAPDH in Rictor cKO compared with control (CNT) at P7, P14, and P30. CNT mean was set to 100% based on averaging of actual numerical values from each Western blot analysis. Data are mean ± SEM. Unpaired *t* test with Welch's correction. Statistical information is given in a table below each corresponding graph and includes age, *n* (written as control and cKO), *p* value, SEM for control, mean of cKO, SEM for cKO, and degrees of freedom (df). Brain or spinal cord sections (P30) were stained with FluoroMyelin. *C*, Corpus callosum in *PDGFRα-Cre; Rictor^fl/fl^* mice had reduced FluoroMyelin signal compared with the corpus callosum in control mice. Scale bar, 500 μm. *D*, *PDGFRα-Cre; Rictor^fl/fl^* spinal cord had no apparent reduction of FluoroMyelin signal compared with control. Scale bar, 500 μm.

sections (65 nm) were mounted on copper grids and viewed at 80 kV on a Tecnai G2 transmission electron microscope (FEI). Electron micrographs of the corpus callosum were imaged near the midline, and spinal cord images were obtained from the region of the dorsal columns. Between 4 and 6 animals were used per genotype per age (indicated as *n* in Fig. 7); and for each animal, between 10 and 12 images were taken and analyzed. g-ratios were determined using AxonDeepSeg (Zaimi et al., 2018) and manual tracing. A myelin/axon mask was generated, and then partial or misidentified objects were manually removed.

Immunofluorescent and fluorescent staining. Mice were anesthetized with isofluorane followed by intraperitoneal injection of avertin or Fatal plus. Intracardial perfusion was performed using phosphate buffered saline (PBS) followed by 4% PFA in PBS with phosphatase inhibitor, 2 mM sodium orthovanadate (Na$_3$VO$_4$, CAS: 13721-39-6). Tissues were dissected and then postfixed in 4% PFA in PBS overnight and transferred to cryoprotect solution (20% glycerol in 0.1 M Sorensen's buffer or 30% sucrose) for at least 72 h. Cervical spinal cord and cortex were cut into 30 or 20 μm free-floating sections and stored in cryostorage solution (30% ethylene glycol, 30% sucrose, 1% PVP-40 in 0.1 M Sorenson's buffer). Before staining, antigen retrieval was performed in 10 mM sodium citrate, pH 6, for 5 min at 65°C (550 W), Pelco Biowave Pro. Sections were permeabilized in 1% Triton X-100 in Tris-buffered saline (TBS) for 10 min at room temperature, washed, and then blocked for 1 h at room temperature with 5% normal donkey serum and 0.3% Triton X-100 in TBS. All other primary antibodies were incubated overnight at 4°C. All secondary antibodies were used at 1:800 concentration and incubated for 45 min at room temperature. All primary and secondary antibody solutions were prepared in 3% normal donkey serum blocking solution. Sections were rinsed with PB and then mounted and coverslipped with Fluoromount-G (Fisher Scientific). For spinal cord analysis, images were acquired in the dorsal column. For corpus callosum, images were acquired at midline in the genu. At least three sections per mouse were imaged.

Mouse OPC isolation and virus treatment. Pups were collected between P0 and P1 from Rictor^fl/fl^ parents. Brains were dissected, and the olfactory bulb and cerebellum were removed. The meninges was removed, and the remaining tissue was mechanically dissociated in DMEM containing Papain and DNase. The resulting mouse mixed glia were grown in OPC media (DMEM with 10% fetal bovine serum (FBS), Penicillin-Streptomycin, 2mM L-glutamine). On day 6 and 8, media was changed to OPC media plus 2.5 μg/mL insulin. On day 10 flasks were then shaken at 100 rpm for 1 h to remove microglia, and then OPCs were shaken off at 225 rpm for 30 h. OPCs were then plated in media containing PDGF and FGF. Forty-eight hours after plating, PDGF/FGF-containing media was replaced with media containing T3 and 500 MOI of either eGFP adenovirus (Vector Biolabs; eGFP adenovirus; catalog #1060; Name: Ad-GFP) or Cre-GFP adenovirus (Vector Biolabs; Cre Recombinase adenovirus; catalog #1710; Name: Ad-Cre-IRES-GFP). Cells were incubated for 72 h and then fixed with 4% PFA.

Microscopy. Fluorescent images were taken on Nikon A1 confocal microscope combined with a Ti2-E microscope with a 20× or 40× objective and a Leica DMi8S with Stellaris 5 with 20× or 63× objective. For each experiment, all microscopy settings were set the same to maintain consistent and comparable images.

Immunofluorescent image analysis. Cell counts using fluorescent images in Figure 2 were done with the automated open source software, Cell profiler (Carpenter et al., 2006). The number of animals used for each analysis defines *n* for each graph, and each animal is a single data point for each graph. Between three and six images were averaged to generate a single data point for each animal. The fluorescent intensity was determined using Fiji open-source software (Schindelin et al., 2012). The immunofluorescent intensity (Figs. 3, 5) was quantified for a 150 μm² ROI within the apparent corpus callosum to generate a mean intensity value, which was normalized relative to the average value of control animals. For Figure 5, the immunofluorescence intensity was measured within the white matter region of the dorsal spinal column. The F-actin to G-actin ratio (see Fig. 9) was generated using a 150 μm² ROI and measuring the F-actin (phalloidin) intensity and the G-actin (DNase I) intensity within that ROI either in corpus callosum or cortex, using "roi-manager" (Fiji). The F-actin intensity measurement was divided by the G-actin intensity measurement.
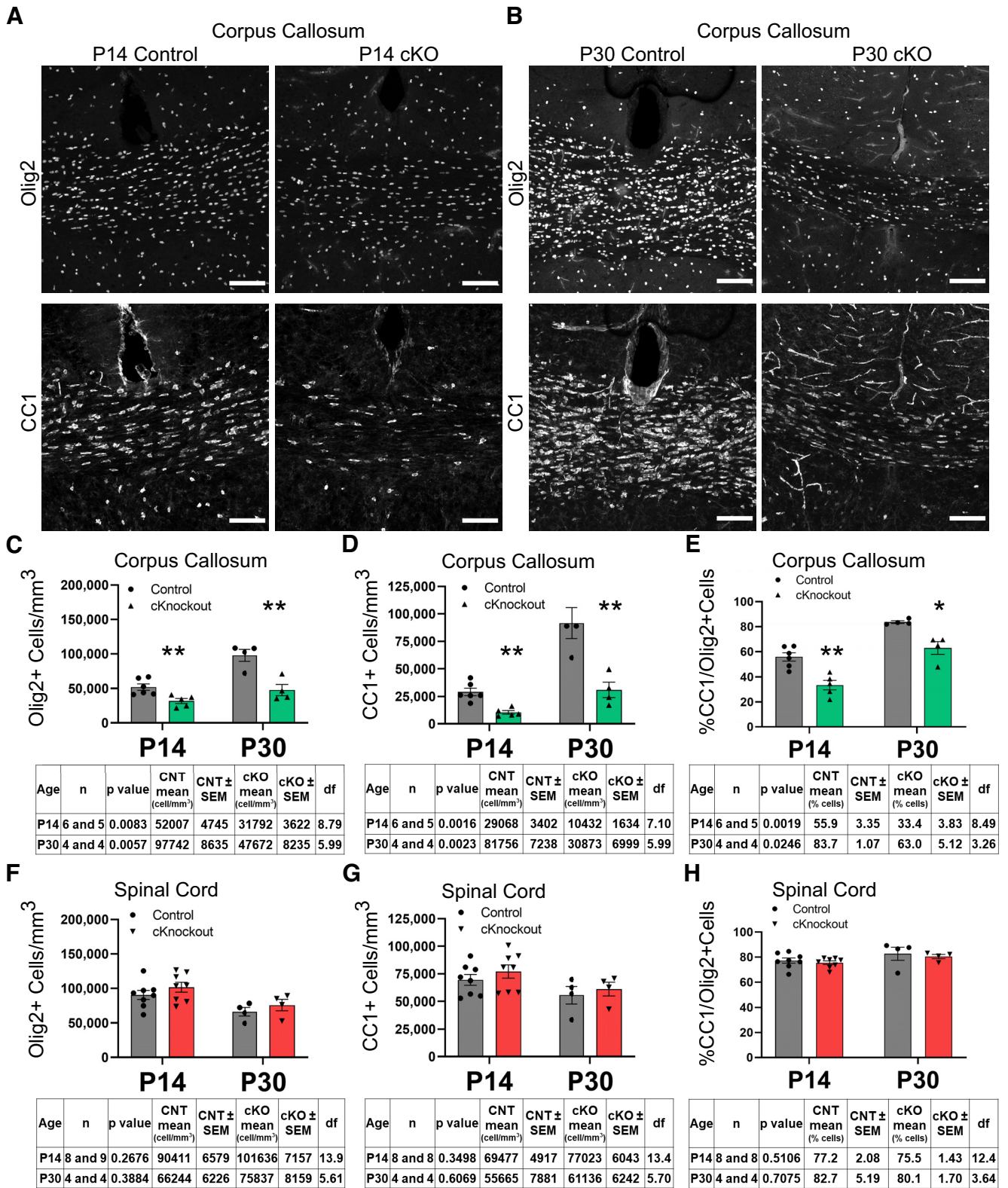
Figure 2. Loss of Rictor from OPCs resulted in decreased total Olig2$^+$ cells and differentiated Olig2$^+$ cells in the corpus callosum but not the spinal cord at P14 and P30. Olig2 and CC1 staining in corpus callosum at P14 (*A*) and P30 (*B*) in control compared with Rictor cKO mice. Scale bar, 100 μm. *C*, Corpus callosum quantification of Olig2$^+$ cells per mm^3. *D*, Corpus callosum quantification of CC1$^+$ cells per mm^3. *E*, Percent of CC1-Olig2 double-positive cells relative to total Olig2$^+$ cells in the corpus callosum. *F*, Spinal cord quantification of Olig2$^+$ cells per mm^3. *G*, Spinal cord quantification of CC1$^+$ cells per mm^3. *H*, Percent of CC1-Olig2 double-positive cells relative to total Olig2$^+$ cells in the spinal cord. Unpaired *t* test with Welch's correction. Statistical information is given in a table below each corresponding graph, including the following: age, *n* (written as control and cKO), *p* value, mean of control, SEM for control, mean of cKO, SEM for cKO, and degrees of freedom (df).
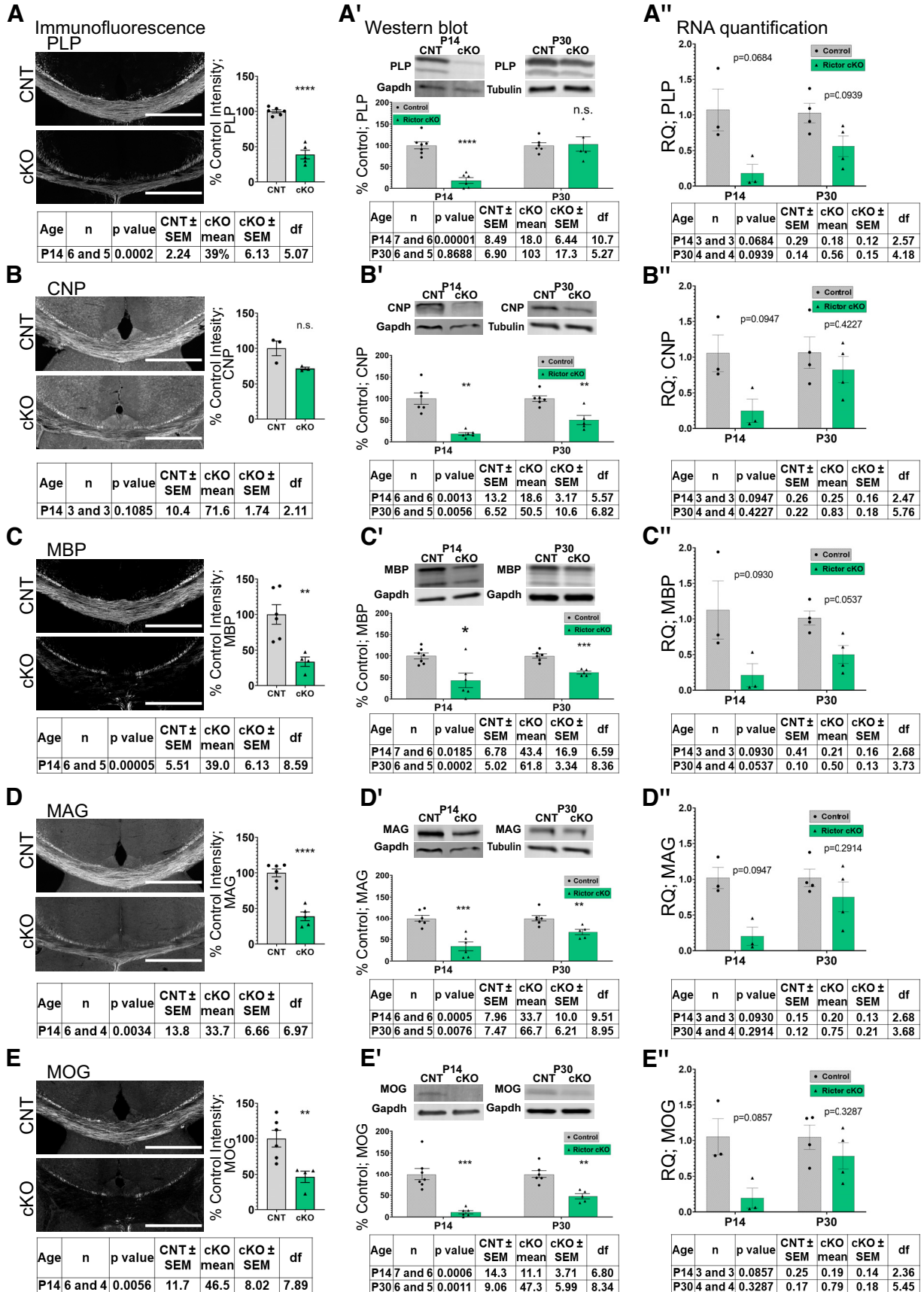
Figure 3. Myelin-specific proteins were decreased in the Rictor cKO corpus callosum compared with control (CNT) through development. *A*, Immunofluorescent (IF) images and quantification at P14 of PLP in the genu of the corpus callosum. *A′*, *A″*, PLP protein (Western blot) and RNA expression (qPCR shown as RQ) in corpus callosum at P14 and P30. *B*, IF images and quantification at P14 CNP in the corpus callosum. *B′*, *B″*, CNP protein (Western blot) and RNA (pPCR) expression in corpus callosum at P14 and P30. *C*, IF images and quantification at P14 MBP in the

Antibodies. Antibodies used for Western blot analysis are as follows: total AKT (AKT (pan) (40D4) anti-mouse, Cell Signaling catalog #2920S, RRID:AB_1147620, 1:500); CNP (Anti-CNPase antibody produced in rabbit, Sigma-Aldrich SKU:C9743, RRID: AB_1840761, 1:1000); GapDH (D16H11; XP Rabbit mAb, Cell Signaling catalog #5174S, RRID:AB_10622025, 1:1000); GapDH (D4C6R; Mouse mAb, Cell Signaling catalog #97166S, RRID:AB_2756824, 1:1000); Gelsolin (Recombinant Anti-Gelsolin antibody [EPR1942], Abcam catalog #ab109014, RRID:AB_10863643, 1:1000); myelin-associated glycoprotein (MAG, D4G3; XP Rabbit mAb, Cell Signaling catalog #9043S, RRID:AB_2665480, 1:1000); MBP (Neuromics catalog #MO22121, RRID:AB_2737143, 1:1000); myelin oligodendrocyte glycoprotein antibody (MOG, Abcam catalog #ab32760, RRID:AB_2145529, 1:1000); total mTOR (7C10; Rabbit mAb, Cell Signaling catalog #2983, RRID:AB_2105622, 1:500); pAkt-S473 (Phospho-Akt (Ser473); D9E XP Rabbit mAb, Cell Signaling catalog #4060S, RRID:AB_2315049, 1:500); pAkt-T308 (Phospho-Akt (Thr308); D25E6 XP Rabbit mAb, Cell Signaling catalog #13038S, RRID:AB_2629447, 1:500); PKCα (D7E6E) Rabbit mAb, Cell Signaling catalog #59754S, RRID:AB_2799573, 1:500; PKC α/β II (Phospho-Thr638/641) anti-Rabbit, Cell Signaling catalog #9375S, Lot 4; RRID:AB_2284224, 1:1000; proteolipid protein (PLP) AA3, RRID:AB_2341144, 1:5000; Phospho-mTOR (Ser2481) Antibody, Cell Signaling catalog #2974, RRID:AB_2262884, 1:500; Phospho-mTOR (Ser2448); D9C2 XP Rabbit mAb, Cell Signaling catalog #5536P, RRID:AB_10691552, 1:500; Recombinant Anti-Profilin 1 antibody [EPR6304], Abcam ab124904, RRID:AB_10975882, 1:1000; Profilin 2 Antibody, Novus catalog #87426, RRID:AB_11007824, 1:250; Phospho-S6 Ribosomal Protein (Ser240/244) Antibody, Cell Signaling catalog #2215S, RRID:AB_331682, 1:500; Rictor Antibody anti-Rabbit, Cell Signaling catalog #2140, RRID:AB_2179961, 1:500; Tubulin (α), Cell Signaling catalog #3873S, RRID:AB_2797891, 1:1000.

Antibodies used in immunofluorescence staining and actin visualization are as follows: CC1 (Anti-APC (Ab-7) Mouse mAb (CC-1), Calbiochem OP80, RRID:AB_2057371, dilution 1:300); MAG (Anti-Myelin Associated Glycoprotein, clone 513 antibody, Millipore mab1567, RRID:AB_2137847, dilution 1:1000); MBP (Neuromics catalog #MO22121, RRID:AB_2737143:, dilution 1:1000); MOG (Abcam catalog #ab32760, RRID:AB_2145529, dilution 1:1000); Olig2 (Anti-Olig2 antibody, Gift from Charles Stiles, RRID:AB_2336877, dilution 1:200; PLP, AA3, RRID:AB_2341144, 1:100); G-Actin (Deoxyribonuclease I, AlexaFluor-594 Conjugate D12372, Molecular Probes, catalog #D12372); F-actin (Cytoskeleton Acti-Stain 488 Phalloidin, catalog #PHDG1-A); Gelsolin (BD Biosciences catalog #610412, RRID:AB_397792); O4 (S. Pfeiffer, Farmington, Connecticut catalog #O4 antibody, RRID:AB_2314991).

qPCR. Corpus callosum and cervical spinal cord samples at P14 and P30 were dissected, submerged in TRIzol (Invitrogen), and stored at −80°C until extraction. Samples were homogenized and RNA extracted. cDNA was generated from 1 µg of RNA using iScript Reverse Transcription Supermix for RT-qPCR (Bio-Rad). Real-time qPCR was performed on a StepOnePlus real-time PCT Machine (Applied Biosystems). Taqman Universal PCR Master Mix (Fisher Scientific) was used with Taqman probes (Fisher Scientific) *gapdh* (Ref 4352661), *Rictor* (Mm01307318_m1), *cnp* (Mm01306641), *mog* (Mm00447824_m1), *mbp* (Mm01266402_m1), *plp1* (Mm01297210_m1), and *mag* (Mm00487538_

m1). All experiments followed the MIQE Guidelines for qPCR (Bustin et al., 2009).

Western blots. The corpus callosum and cervical spinal cord of P7, P14, and P30 animals were dissected, snap-frozen in liquid nitrogen, and stored at −80°C until lysis. The corpus callosum of aged animals between 20 and 50 weeks were dissected and frozen the same way. The tissue was lysed in a glass homogenizer in cold RIPA buffer (Sigma-Aldrich) with a phosphatase inhibitor cocktail (Calbiochem; Millipore) and protease inhibitor tablet (complete-mini; Roche). The crude lysates were centrifuged at $10,000 \times g$ for 10 min at 4°C. The supernatants were then collected, and the protein concentration was determined using the BCA protein Assay Kit (Fisher Scientific). The lysates were then resolved using 4%-20% SDS-PAGE gradient gels and transferred to PVDF membranes. The membranes were blocked with 5% BSA in TBS and then incubated with primary antibodies overnight at 4°C. Immunodetection was performed using IRDye infrared secondary antibodies (LI-COR). All blots were scanned and quantified using an Odyssey Infrared imager (LI-COR) and Image Studio Lite software (version 5.2).

Experimental design and statistical analysis. All statistical analyses were done using GraphPad Prism version 9.3.1 for Windows, GraphPad Software (www.graphpad.com). When testing significance between the cKO and control sample, we used unpaired t test with Welch's correction to account for variability in the SD. In Figure 7, we analyzed total axon diameter by g-ratio and performed a simple linear regression for the graphs. Figure 7 also included a histogram analysis of the relative frequency, in which we used frequency distribution tabulated as relative frequency in percentages with a bin width of 0.5. In Figure 8, when testing the significance between cortex staining and corpus callosum staining, a paired t test was used to account for batch variability. Statistical significance was defined as $p < 0.05$. When error bars are shown, they are reported as mean $\pm$ SEM.

Data access. Data are made available (Oct. 24, 2022) at www.osf.io/qndbm for PDGFRapha_Rictor generated by K.D.D., A.R.A. and L.T.F.

Results

CNS region-specific myelin deficiency in PDGFRα-Cre; Rictor^fl/fl mice

To investigate the role of mTORC2 signaling in OPC myelination, we crossed PDGFRα-Cre mice with Rictor^fl/fl mice to generate *PDGFRα-Cre; Rictor^{fl/fl}* mice (Rictor cKO mice). Rictor expression was significantly reduced at all ages, P7, P14, and P30, in brain (Fig. 1A) and spinal cord (Fig. 1B). We confirmed that the KO of Rictor was specific to OPCs with a combination of FACS and RT-PCR (see Materials and Methods). We stained tissue with FluoroMyelin and determined by qualitative analysis that the brain from postnatal day 30 (P30) Rictor cKO mice and Rictor^fl/fl littermate controls appeared to have a dramatic reduction of myelin, but there was little reduction in spinal cord (Fig. 1C,D), suggesting a region-specific requirement of mTORC2 in PDGFRα-expressing OPCs. This qualitative assessment of myelin changes was extensively characterized in further studies.

Rictor loss reduced oligodendrocyte differentiation in corpus callosum but not spinal cord

Since Rictor deletion in OPCs apparently reduced myelin in corpus callosum but not spinal cord (Fig. 1), it was important to test whether OPC differentiation was affected in corpus callosum or spinal cord. We quantified the number of total oligodendrocytes in Rictor cKO mice by counting the total number of Olig2$^+$ oligodendrocyte lineage cells per mm^3 (Fig. 2C,F). We quantified the number of differentiated oligodendrocytes by counting the total number of CC1$^+$ cells per mm^3 (Fig. 2D,G). The proportion of CC1$^+$ cells to Olig2$^+$ cells was determined by the relative percentage of CC1$^+$ cells among total Olig2$^+$ oligodendrocytes. In

corpus callosum. ***C′***, ***C′′***, MBP protein (Western blot) and RNA (qPCR) expression in corpus callosum at P14 and P30. ***D***, IF images and quantification at P14 MAG in the corpus callosum. ***D′***, ***D′′***, MAG protein (Western blot) and RNA (qPCR) expression in corpus callosum at P14 and P30. ***E***, IF images and quantification at P14 MOG in the corpus callosum. ***E′***, ***E′′***, MOG protein (Western blot) and RNA (qPCR) expression in corpus callosum at P14 and P30. CNT mean was set to 100% based on averaging of actual numerical values for IF and Western blot. Data are mean $\pm$ SEM. Unpaired t test with Welch's correction. Statistical information is given in a table below each corresponding graph and includes age, n (written as control and cKO), p value, SEM for control, mean of cKO, SEM for cKO, and degrees of freedom (df). Scale bar, 500 µm.

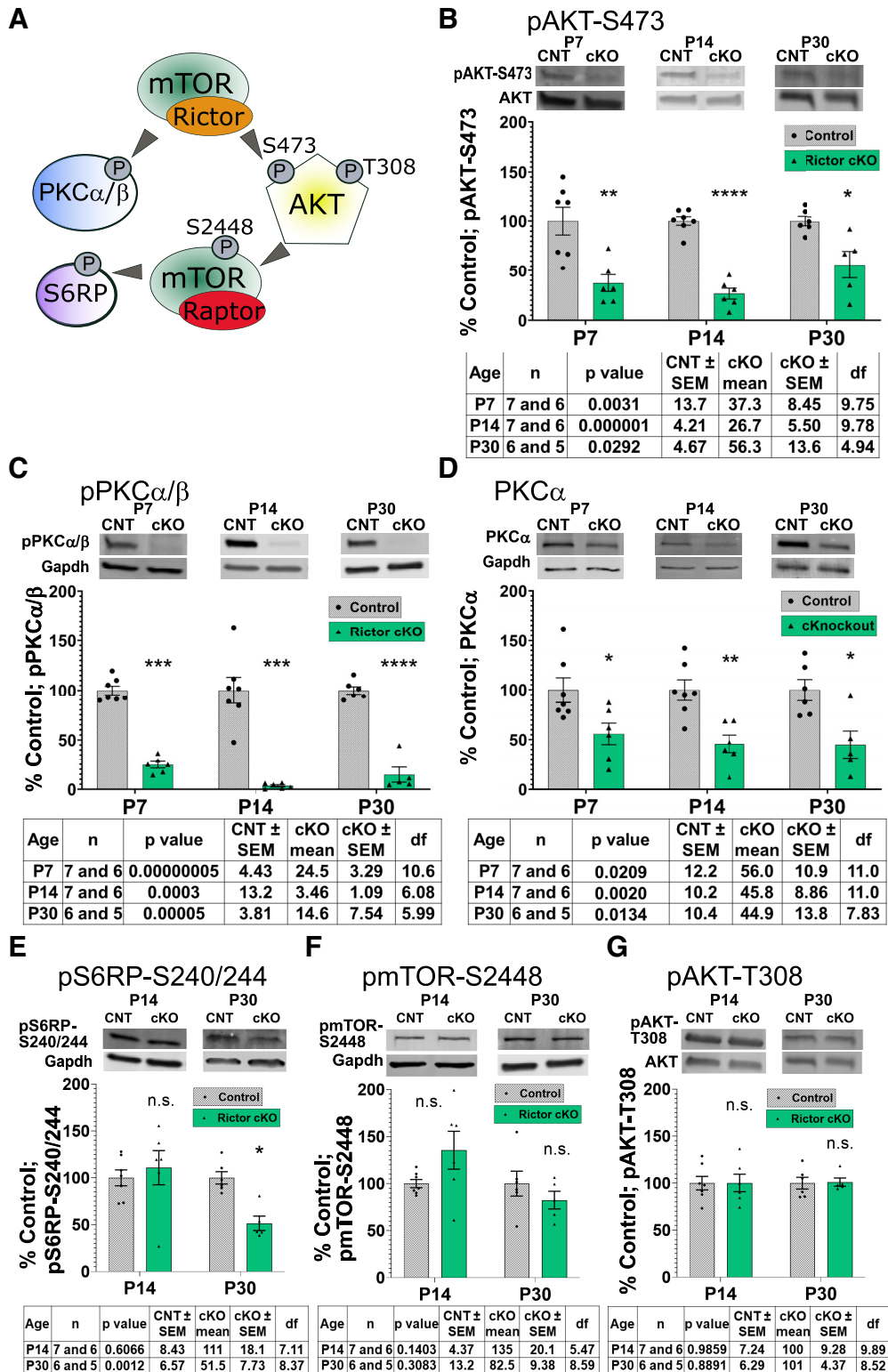**Figure 4.** mTORC2 signaling was reduced in the corpus callosum of Rictor cKO mice through development. **A**, Model of mTORC2 interaction with substrates in the mTOR pathway. **B–G**, Western blots of mTORC1 and mTORC2 substrates. **C, D**, Western blot of phosphorylated mTORC2 substrates of ages P7, P14, and P30. **B**, pAKT-S473 normalized to total AKT. **C**, pPKCα/β normalized to GapDH. **D**, Total PKCα normalized to GapDH. **E–G**, Western blot of phosphorylated non-mTORC2 substrates. **F**, pS6RP normalized to GapDH. **G**, pmTOR-S2448 normalized to GapDH. **H**, pAKT-T308 normalized to total AKT. Unpaired t test with Welch's correction. Statistical information is given in a table below each corresponding graph and includes age, n (written as control and cKO), p value, SEM for control, mean of cKO, SEM for cKO, and degrees of freedom (df).

the corpus callosum, there was a statistically significant decrease in the total number of Olig2$^+$ cells in Rictor cKO mice at P14, compared with control, which was further decreased by P30 (Fig. 2C). The total number of CC1$^+$ cells was significantly decreased

in the Rictor cKO mice at P14 and P30 compared with control. Additionally, the percentage of those cells that differentiated to CC1$^+$ cells was significantly reduced in corpus callosum at P14 and P30 (Fig. 2D). Thus, the relative number of oligodendrocyte
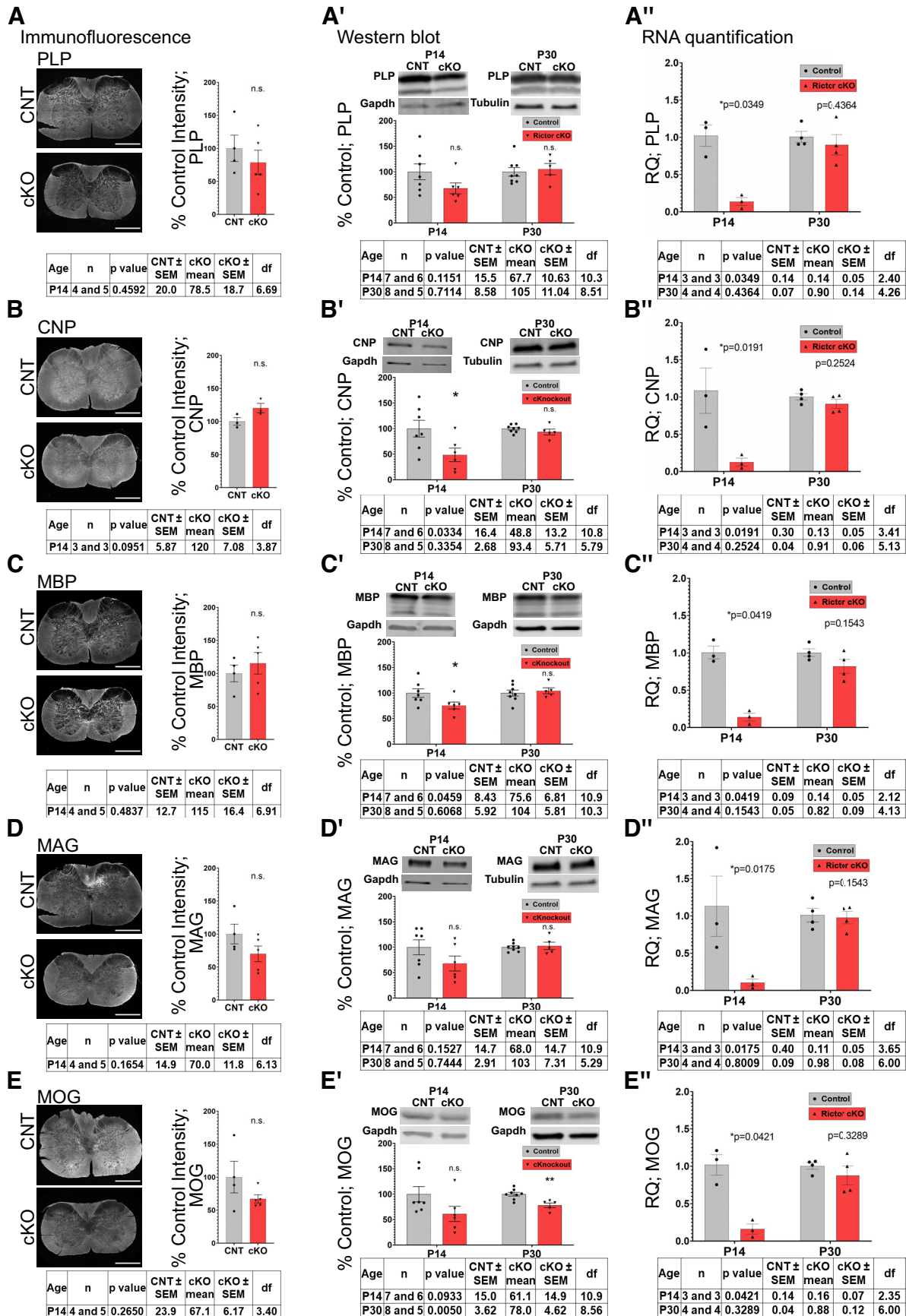
Figure 5. Myelin-specific proteins were similar in Rictor cKO and CNT spinal cord through development. ***A***, Immunofluorescent (IF) images and quantification of dorsal spinal column at P14 of PLP in the spinal cord. ***A′***, ***A″***, PLP protein (Western blot) and RNA (qPCR as shown by RQ) expression in spinal cord at P14 and P30. ***B***, IF images and quantification of dorsal spinal column at P14 CNP in the spinal cord. ***B′***, ***B″***, CNP protein (Western blot) and RNA expression (qPCR) in spinal cord at P14 and P30. ***C***, IF images and quantification of dorsal spinal column at P14

lineage cells that were differentiating to CC1$^+$ cells was initially only ~50% of the low number of total Olig2$^+$ cells at P14. By P30, the percentage of Olig2$^+$ cells that were differentiating was still significantly reduced at ~60% for Rictor cKO compared with 80% for control animals. Thus, deletion of Rictor from corpus callosum OPCs resulted in the decreased number of both Olig2$^+$ cells and differentiated Olig2$^+$ cells resulting in decreased myelin in the corpus callosum at P30 in Figure 1. As expected, in spinal cord, where myelination in the Rictor cKO appeared to be similar to control, there was no change in the total number of Olig2$^+$ cells at either age (Fig. 2F), and no change in the total number or in the percentage of CC1$^+$ cells among oligodendrocytes in Rictor cKO mice compared with control (Fig. 2F,G).

Decreased myelin gene expression following Rictor deletion from OPCs

We hypothesized that the loss of mTORC2 signaling would result in decreased myelin protein expression in the corpus callosum consistent with the decreased FluoroMyelin staining (Fig. 1) and reduced oligodendrocyte number and differentiation (Fig. 2). We therefore investigated myelin protein and mRNA expression in corpus callosum (Fig. 3). All myelin-specific proteins studied (i.e., PLP, CNP, MAG, MOG, and MBP) were significantly decreased in Rictor cKO mice compared with control at P14, by Western blot analysis (Fig. 3). Immunofluorescence images of brain sections were quantified at P14, establishing a statistically significant decrease in mean intensity for all myelin proteins except CNP, which was decreased compared with control but did not meet the standard for statistical significance (Fig. 3B). By Western blot, all myelin proteins were reduced at P14; CNP, MAG, MOG, and MBP protein levels were still reduced at P30 (Fig. 3B′-E′), although PLP protein level had recovered (Fig. 3A′). Thus, the impact of the loss of mTORC2 signaling in corpus callosum oligodendrocytes extended into early adulthood, with some myelin-specific proteins, such as PLP, recovering in P30 animals.

Because mTOR can regulate both protein translation and RNA transcription, it was important to establish whether the decreased myelin proteins in the Rictor cKO mice resulted from reduced myelin RNAs. qPCR of Rictor cKO and control tissue established that myelin mRNAs were reduced in the Rictor cKO mice compared with control at P14. However, given sample variability, the differences were not significant (Fig. 3A′-E′). At P30, myelin mRNA levels approached control levels in the Rictor cKO corpus callosum. Thus, the loss of myelin proteins in the Rictor cKO corpus callosum likely resulted from decreased mRNA abundance, at least at P14, but there was recovery with time. Together, these data demonstrate that loss of mTORC2 signaling reduces oligodendrocyte differentiation and consequently myelin gene expression in the corpus callosum during development.

←

MBP in the spinal cord. *C′*, *C′′*, MBP protein (Western blot) and RNA expression (qPCR) in spinal cord at P14 and P30. *D*, IF images and quantification of dorsal spinal column at P14 MAG in the spinal cord. *D′*, *D′′*, MAG protein (Western blot) and RNA expression (qPCR) in spinal cord at P14 and P30. *E*, IF images and quantification of dorsal spinal column at P14 MOG in the spinal cord. *E′*, *E′′*, MOG protein (Western blot) and RNA expression (qPCR) in spinal cord at P14 and P30. CNT mean set to 100% based on averaging of actual numerical values for IF and Western blot. Data are mean ± SEM. Unpaired *t* test with Welch's correction. Statistical information is given in a table below each corresponding graph and includes age, *n* (written as control and cKO), *p* value, SEM for control, mean of cKO, SEM for cKO, and degrees of freedom (df). Scale bar, 500 μm.

Decreased mTORC2 signaling in Rictor cKO mice

It was important to establish whether Rictor cKO mice had reduced mTORC2 signaling in regions with reduced myelin. As noted above, Rictor protein expression was significantly reduced at P7, P14, and P30 in Rictor cKO corpus callosum (Fig. 1A), establishing effective deletion of Rictor. Signaling through the mTORC2 complex (Fig. 4A) was investigated to determine whether the deletion of Rictor resulted in a loss of mTORC2 signaling. We analyzed the phosphorylation of mTORC2 specific substrates Akt-S473 and PKCα/β in Rictor cKO and control corpus callosum, and both were significantly decreased in Rictor cKO mice at P7, P14, and P30 (Fig. 4B,C). We also measured the total protein levels of PKCα and found that the levels of total PKCα were significantly decreased at all ages (Fig. 4D), which may account for some, but likely not all, of the decreased pPKCα/β (Fig. 4C). Thus, through development, Rictor cKO mice had reduced mTORC2 signaling in corpus callosum.

Because mTORC2 functions within the larger mTOR signaling pathway (Fig. 4A), we investigated whether other parts of that pathway were impacted by the loss of mTORC2 signaling. No significant change in the total protein levels of Akt, mTOR, or S6RP was noted in young mice (Fig. 4B,G, loading controls), although when quantified at P30, total Akt was reduced by 13% (quantification not shown). Phosphorylation at pAkt-T308 and pmTOR-S2448 were unaffected at P14 and P30 (Fig. 4F,G). Thus, initial activation of Akt from upstream signaling (pAkt-T308) was normal, as was mTOR phosphorylation normally regulated by mTORC1 (Copp et al., 2009). Downstream signaling through mTORC1 was initially unaffected (i.e., there was no significant reduction of pS6RP at P14; Fig. 4E). Interestingly, however, at P30 pS6RP was decreased in Rictor cKO corpus callosum compared with control (Fig. 4E). Together, these data indicate that the loss of mTORC2 signaling did not initially impact major mTORC1 signaling, although the loss of pS6RP by P30 may result from the overall impact of mTORC2 loss on the number of differentiating oligodendrocytes in corpus callosum.

Impact of mTORC2 loss in spinal cord OPCs

Our initial FluoroMyelin staining showed that Rictor loss in OPCs had no noticeable effect on spinal cord myelination (Fig. 1), or oligodendrocyte differentiation (Fig. 2), suggesting region-specific mTORC2 signaling. It was important to next assess myelin gene expression and mTORC2 signaling in Rictor cKO spinal cord. By immunofluorescence, the myelin proteins in the white matter of the dorsal column of cervical spinal cord, from Rictor cKO mice, were not significantly changed, relative to control spinal cord. When quantified by Western blot, PLP and MAG protein were not significantly changed in Rictor cKO cervical spinal cord, compared with control at either P14 or P30 (Fig. 5A′,D′). By contrast, CNP and MBP protein levels were initially significantly decreased in Rictor cKO spinal cord relative to P14 controls, and MOG protein was somewhat reduced at P14. This apparent difference likely results from analysis of one region of spinal cord by immunofluorescence relative to Western blots of a large portion of spinal cord. By P30, however, CNP and MBP were no longer decreased; but interestingly, MOG protein was significantly decreased in Rictor cKO spinal cord compared with control at P30. While the myelin protein levels at P14 were somewhat reduced, the RNAs for all these proteins were dramatically reduced at P14 in Rictor cKO spinal cord relative to controls (Fig. 5A′′-E′′). However, these myelin RNAs had all recovered to control levels by P30 in this tissue.
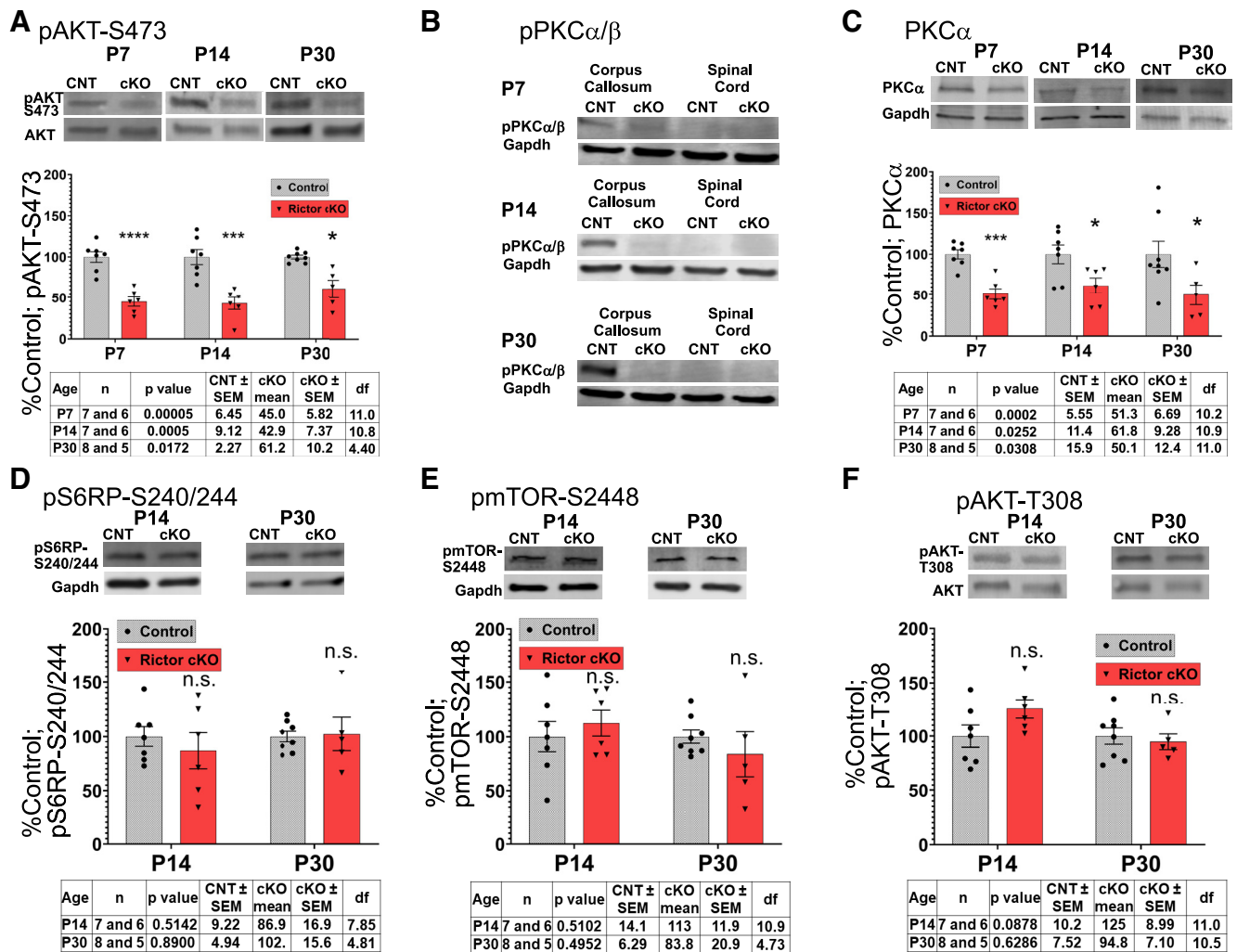
Figure 6. mTORC2 signaling was reduced in the Rictor cKO spinal cord through development. **A**, pAKT-S473 normalized to total AKT in cKO compared with CNT at ages P7, P14, and P30. **B**, pPKCα/β in corpus callosum compared with spinal cord at ages P7, P14, and P30. **C**, Total PKCα normalized to GapDH at ages P7, P14, and P30. **D**, pS6RP normalized to GapDH at P14 and P30. **E**, pmTOR-S2448 normalized to GapDH at P14 and P30. **F**, pAKT-T308 normalized to total AKT at P14 and P30. CNT mean set to 100% based on averaging of actual numerical values. Data are mean ± SEM. Unpaired *t* test with Welch's correction. Statistical information is given in a table below each corresponding graph and includes age, *n* (written as control and cKO), *p* value, SEM for control, mean of cKO, SEM for cKO, and degrees of freedom (df).

Given the apparently differential impact of Rictor loss in developing OPCs in spinal cord relative to corpus callosum, we investigated mTORC2 signaling in developing spinal cord. As in corpus callosum, there was a significant decrease in Rictor protein levels in the spinal cord of Rictor cKO mice (Fig. 1*B*) at P7, P14, and P30, and a decrease in the mTORC2 signaling substrate pAkt (S473) (Fig. 6*A*). We were surprised to find that neither control nor Rictor cKO spinal cord had detectable signal for phosphorylation of the mTORC2 substrate pPKCα/β (Fig. 6*B*). To confirm its absence in spinal cord, we compared pPKCα/β expression in corpus callosum and spinal cord from P7 to P30 (Fig. 6*B*). As expected, significant expression was noted in control corpus callosum at all ages, and it was reduced in Rictor cKO corpus callosum. However, at no time during development was pPKCα/β detected in control or Rictor cKO spinal cord. Total PKCα was significantly decreased in the Rictor cKO compared with control (Fig. 6*C*). However, as we did not observe any pPKCα/β in either the control or cKO spinal cord, this decrease in total PKCα protein would not likely impact signaling. As in Rictor cKO corpus callosum, there was no significant change in mTORC1 specific substrates in the spinal cord (Fig. 6*D–F*),

including pS6RP, which was reduced in P30 Rictor cKO corpus callosum (Fig. 4*E*), and which we hypothesized may result from the overall reduction in oligodendrocyte differentiation/myelination in corpus callosum (Fig. 2). Total levels of Akt, mTOR, and S6 were measured; only total mTOR at P30 was significantly decreased by 38% (data not shown). These data confirm the loss of Rictor protein and of classical mTORC2 signaling in the spinal cord of Rictor cKO mice. Importantly, despite this, few significant myelin losses were noted during Rictor cKO spinal cord development (Fig. 5). These data further demonstrate significant differences in the mTORC2 signaling requirements for corpus callosum and spinal cord oligodendrocytes, and they highlight phospho-PKCα/β as a potentially important differential mediator of mTORC2 signaling, functioning in corpus callosum and not in spinal cord.

Impact of Rictor loss in developing oligodendrocytes on the number of myelinated axons

Ablation of mTORC2 signaling in OPCs reduced differentiation of OPCs to CC1^{+} maturing oligodendrocytes and overall myelin production in corpus callosum to a much greater extent than in
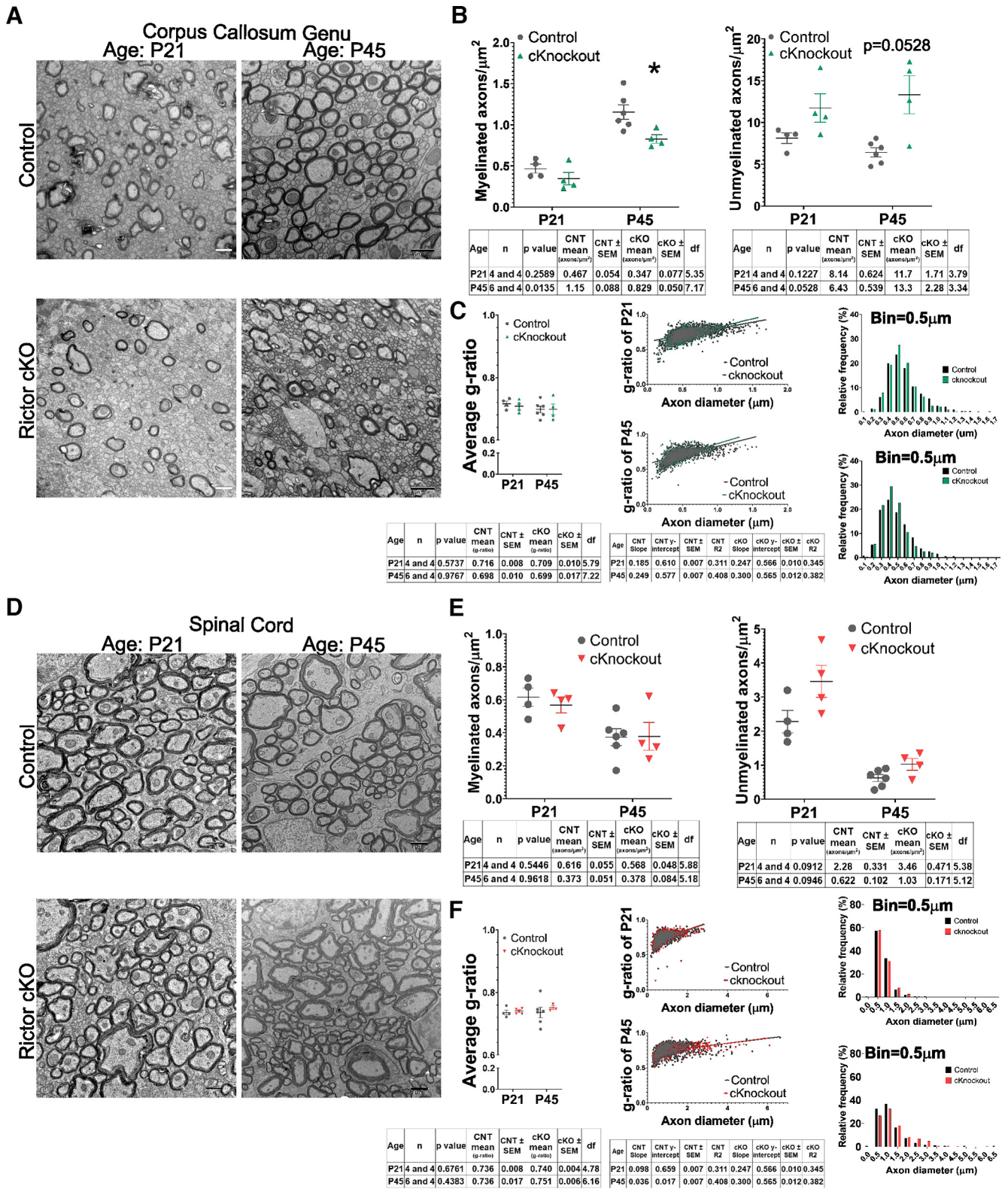
Figure 7. Loss of Rictor resulted in regional differences in the number of myelinated axons and unmyelinated axons when analyzing the corpus callosum and spinal cord. *A*, Transmission electron microscopy (TEM) images of the corpus callosum (genu) at P21 and P45 in Rictor cKO compared with control (CNT). *B*, Quantification of myelinated and unmyelinated axons in TEM images. Left, Myelinated axons per μm^2 P21 and P45. Right, Unmyelinated axons per μm^2 P21 and P45. *C*, Quantification of g-ratio of myelinated axons in TEM images. Left, P21 average g-ratio; P45 average g-ratio. Middle, Distribution of g-ratio by axon diameter (μm). P21 and P45 simple linear regression. Right, Relative frequency percent of myelinated axon diameters for P21 and P45 in the corpus callosum for control and Rictor cKO mice. Bin, 0.5 μm. *D*, TEM images of the Rictor cKO spinal cord compared with control at ages P21 and P45. *E*, Quantification of myelinated and unmyelinated axons of TEM images. Left, Myelinated axons per μm^2 P21 and P45. Right, Unmyelinated axons per μm^2 P21 and P45. *F*, Quantification of g-ratio of myelinated axons in EM images. Left, P21 average g-ratio; P45 average g-ratio. Middle, Distribution of g-ratio by axon diameter (μm). P21 and P45 simple linear regression. Right, Relative frequency percent of myelinated axon diameters for P21 and P45 in the spinal cord for control and Rictor cKO mice. Data are mean ± SEM. Unpaired *t* test with Welch's correction or simple linear regression. Statistical information is given in a table below each corresponding graph and includes age, *n* (written as control and cKO), *p* value, SEM for control, mean of cKO, SEM for cKO, and degrees of freedom (df). Scale bar: TEM images, 1 μm.
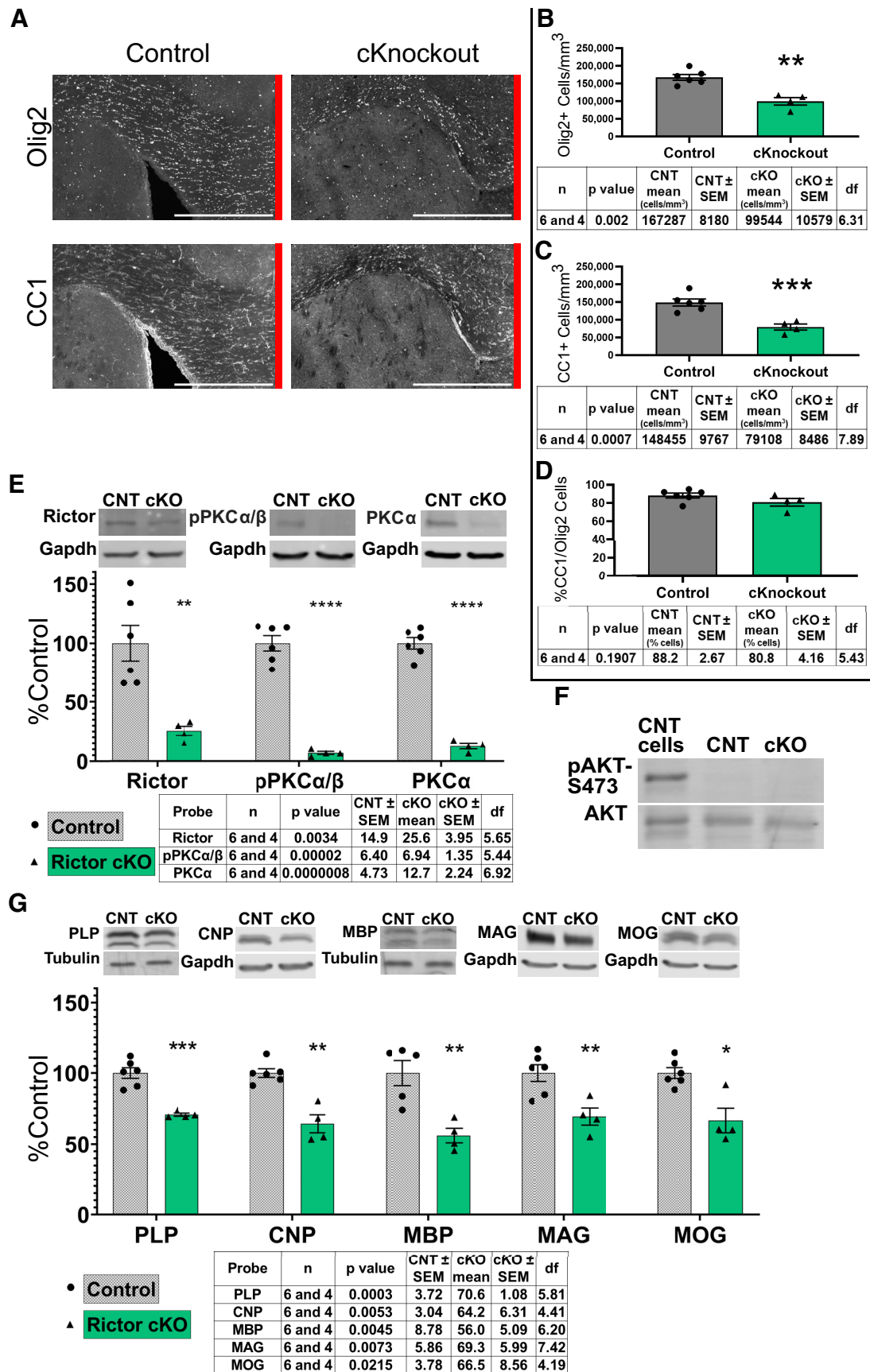
Figure 8. Reduced oligodendrocyte lineage cells and myelin proteins persisted in Rictor cKO animals aged 20-50 weeks. *A*, Olig2 and CC1 staining in corpus callosum in aged mice in control compared with Rictor cKO mice. Red bar represents the midline of the corpus callosum. Scale bar, 500 μm. *B*, Olig2$^+$ cells per mm^3 in corpus callosum of aged animals. *C*, CC1$^+$ cells per mm^3 in corpus callosum of aged animals. *D*, Percent of CC1-Olig2 double-positive cells among total Olig2$^+$ cells in the corpus callosum in aged animals. Statistical information is given in a table

spinal cord. We therefore studied how myelination of individual axons was impacted in corpus callosum and spinal cord by electron microscopy at P21 and P45 (Fig. 7). The density of myelinated axons in Rictor cKO corpus callosum genu at P21 was not significantly reduced; however, at P45, the density of myelinated axons was significantly reduced. The density of unmyelinated axons was increased at P45; but given high variability among the Rictor cKO samples, the increase was not statistically significant ($p = 0.0528$) (Fig. 7A,B). Nevertheless, despite the significant reduction in myelinated axons in Rictor cKO corpus callosum, the total number of axons was somewhat increased in Rictor cKO corpus callosum (P21 control: mean = 8.60 axons per μm^2; P21 cKO: mean = 12.08 axons per μm^2, $p = 0.1337$; P45 control: mean = 7.58 axons per μm^2; P45 cKO: mean = 14.15 axons per μm^2, $p = 0.0583$). Importantly, when g-ratios, a standard measure of myelin thickness, were quantified at either P21 or P45, the g-ratios for Rictor cKO or control corpus callosum myelinated axons were comparable, indicating that, while fewer axons were myelinated, those that were myelinated had normal myelin thickness (Fig. 7C). The relative frequency distribution of the diameter of myelinated axons shows a slight shift to reduced diameter axons in the Rictor cKO corpus callosum compared with control for both P21 and P45.

By contrast, no significant change in the density of myelinated or unmyelinated axons in Rictor cKO spinal cord was noted at either P21 or P45, relative to controls (Fig. 7D,E). As with Rictor cKO corpus callosum, there was no significant change in g-ratios of myelinated axons in the spinal cord of Rictor cKO mice relative to control (Fig. 7F). The relative frequency distribution of axon diameters in the spinal cord showed no difference in the Rictor cKO compared with control at P21 and P45.

Older Rictor KO animals continued to have fewer oligodendrocyte lineage cells and reduced myelin proteins
Earlier studies of Rictor conditional deletion in oligodendrocyte lineage cells suggested that the impact of Rictor loss was a delay in differentiation (Grier et al., 2017). Therefore, to determine whether Rictor cKO mice in the current study could recover myelin over a longer time period, we collected older animals. The Rictor cKO mice died young, but ~4 mice survived to older ages, and we analyzed mice between the ages of 20 and 50 weeks as a group (approximately P140 and P350). Corpus callosum tissue was analyzed by immunofluorescence for oligodendrocyte numbers and by Western blot for protein levels. We quantified the total Olig2$^+$ and CC1$^+$ cells per mm^3 and both remained significantly decreased in the Rictor cKO mice compared with controls (Fig. 8A–C). The percentage of CC1$^+$/Olig2$^+$ cells, however, was not significantly different (Fig. 8D), indicating that while the percent of differentiating oligodendrocytes recovered close to control levels, the Rictor cKO animals did not recover the deficit in total Olig2$^+$ cells or differentiating Olig2$^+$ cells in corpus callosum over time.

←

below each corresponding graph and includes n (written as control and cKO), p value, mean of control, SEM for control, mean of cKO, SEM for cKO, and degrees of freedom (df). **E**, Western blot analysis and quantification of Rictor protein, phospho-PKCα/β, and PKCα proteins comparing control and Rictor cKO aged mice. **F**, Western blot analysis of phospho-AKT-S473 levels comparing oligodendrocyte lineage cells cultured in vitro (positive control) to control and Rictor cKO corpus callosum of aged mice, establishing loss of pAkt-S473 in aged control corpus callosum. **G**, Western blot analysis and quantification of PLP, CNP, MBP, MAG, and MOG myelin proteins comparing control and Rictor cKO aged mice. Statistical information is given in a table below each corresponding graph and includes age, n (written as control and cKO), p value, SEM for control, mean of cKO, SEM for cKO, and degrees of freedom (df).

The Rictor, pPKCα/β, and PKCα protein levels were also significantly lower in the Rictor cKO mice compared with controls (Fig. 8E). Interestingly, pAKT-S473 was undetectable in either the control or Rictor cKO aged animals (Fig. 8F). These data may suggest that signaling through pAKT-S473 in the corpus callosum may not occur as mice age. PLP, CNP, MBP, MAG, and MOG were all significantly decreased in the Rictor cKO aged animals (Fig. 8G). These data together indicate that, in the corpus callosum of PDGFRα-Cre driven Rictor cKO animals, there was no recovery of the hypomyelination observed in early development.

Rictor conditional deletion results in altered actin cytoskeleton regulators
An important downstream target of mTORC2 signaling is the cytoskeleton, specifically actin (Oh and Jacinto, 2011). Several models of active myelination indicate that the cycling of F-actin and G-actin is involved in the production of myelin, and as oligodendrocytes myelinate, the amount of G-actin increases and F-actin decreases (Nawaz et al., 2015; Zuchero et al., 2015). A tissue stain allows quantification of the F-actin/G-actin ratio (Nawaz et al., 2015); and as expected, the F-actin/G-actin ratio was higher in gray matter areas than white matter areas (Fig. 9A–D; i.e., in cortex relative to corpus callosum) at both P14 and P30. In order to assess whether there was any change in the F-actin/G-actin ratio induced by loss of mTORC2 signaling in corpus callosum oligodendrocytes, the F-actin/G-actin ratio was compared; but in the Rictor cKO mice, that ratio was comparable to control. Interestingly, this analysis also highlighted the reduction in the overall width of the corpus callosum in the Rictor cKO mice compared with control at P14 and P30 (Fig. 9E). This likely resulted from the reduction in myelinated axons in corpus callosum of Rictor cKO mice (Fig. 7).

Despite the comparable ratio of F-actin/G-actin, there were important differences in some regulators of actin polymerization in the Rictor cKO mice. When quantified by Western blot, profilin1 was somewhat reduced through development in Rictor cKO corpus callosum, while profilin2 was unchanged, and these actin regulators were only minimally reduced in Rictor cKO spinal cord (Fig. 8H–K). Importantly, gelsolin was dramatically reduced in Rictor cKO corpus callosum even in the older (P140-P350) mice. By contrast, despite the loss of mTORC2 signaling in spinal cord of Rictor cKO mice (Fig. 9G), gelsolin was not significantly affected in the spinal cord of Rictor cKO mice. These data suggest that gelsolin regulation of actin depolymerization may be a downstream effector of mTORC2 signaling, but that the mTORC2 impact on gelsolin regulation of the cytoskeleton was regional, and occurred preferentially in the corpus callosum, but not in spinal cord.

***In vitro* Rictor KO results in impaired oligodendrocyte differentiation**
To investigate whether the impairment of oligodendrocyte differentiation observed in P14 and P30 Rictor cKO animals (Fig. 2) could be recapitulated in vitro, mOPCs from Rictor$^{fl/fl}$ animals were cultured and transduced with adenovirus expressing either GFP only or GFP and Cre, to delete Rictor. Cells were collected between 3 and 4 d after treatment with virus. Samples were labeled with Olig2 to ensure that green cells were oligodendrocyte lineage cells and differentiation was assessed using O4, which labels differentiating cells but not OPCs (Fig. 10). Some morphologic alteration of transduced cells was noted even in GFP-only transduced cells (Fig. 10A, green cells, top row). However, Cre
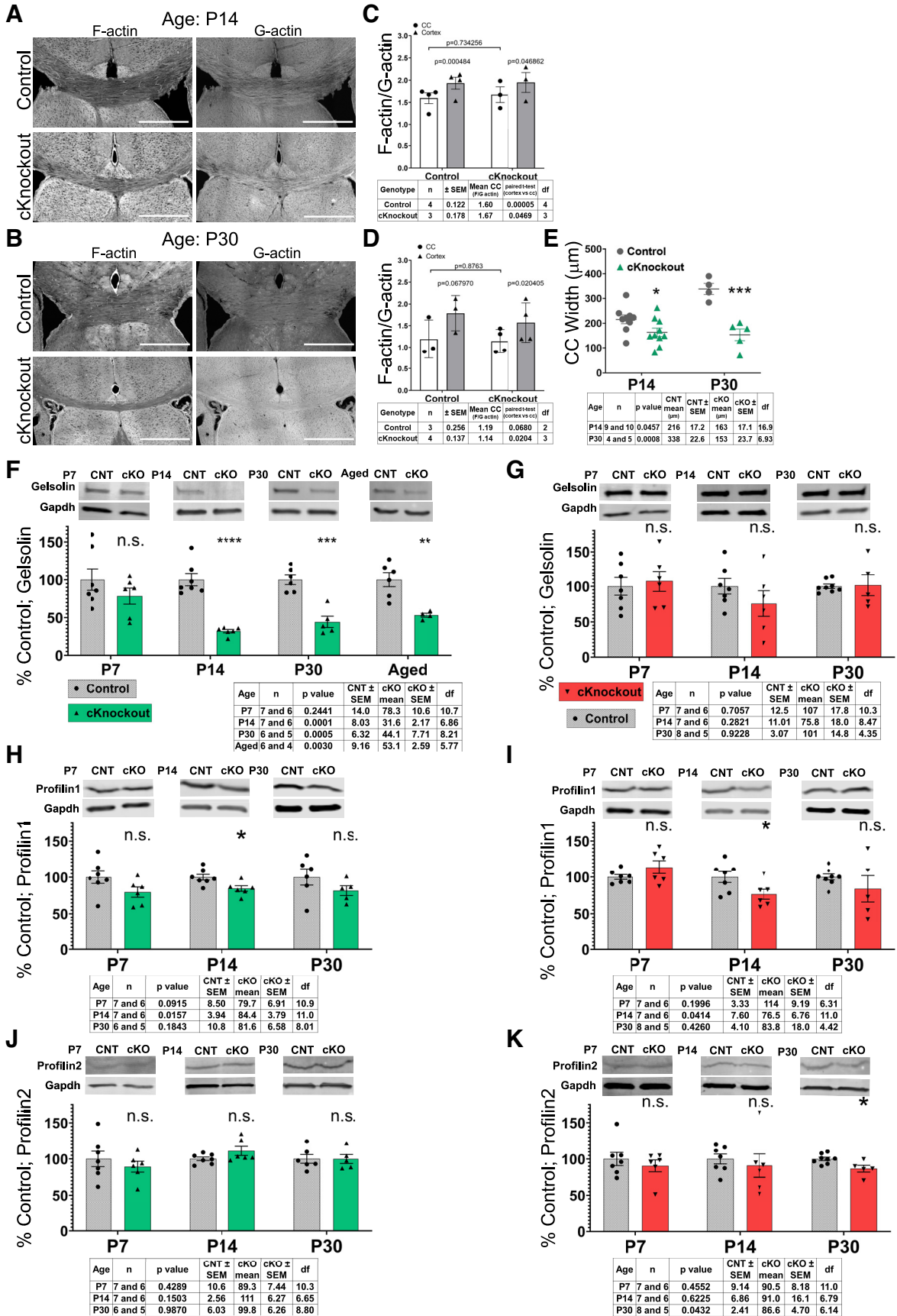
Figure 9. Loss of mTORC2 signaling had little impact on G-actin/F-actin ratio in corpus callosum but resulted in decreased gelsolin. **A**, Corpus callosum of P14 animals stained for F-actin (phalloidin) and G-actin (DNase I), comparing Rictor cKO mice with control. Scale bar, 500 μm. **B**, Corpus callosum of P30 animals stained for F-actin and G-actin comparing Rictor cKO with control. Scale bar, 500 μm. **C**, Ratio of F-actin to G-actin intensity at age P14 in white matter (open bars) or gray matter (gray bars). **D**, Ratio of F-actin to G-actin intensity at age P30 in white

expression dramatically altered OPC differentiation (Fig. 10A′, A″). Strikingly, essentially zero Cre-treated cells differentiated to express O4 (Fig. 10B), which suggests that the loss of mTORC2 signaling impaired OPC differentiation (the only O4$^+$ cell present among 806 cells analyzed is in Fig. 10A″). Cre-expressing cells had more rounded morphology with fewer processes compared with control GFP-expressing cells. These data precluded extensive investigation of later stages of oligodendrocyte differentiation; but having noted that gelsolin was reduced in Rictor cKO corpus callosum (Fig. 9), we investigated the impact of mTORC2 loss on gelsolin expression in cultured OPCs (Fig. 10C). The distribution of the gelsolin in Cre-treated OPCs (Fig. 10C″,C‴,C⁗) was dramatically altered; it was more uniform than in control GFP-expressing cells (Fig. 10C,C′), which had concentrated gelsolin signal in processes, including at the tips. These data would indicate that the loss of Rictor in cultured OPCs reduced their ability to differentiate, and that it may induce morphologic changes that include altered gelsolin localization.

Discussion

The production of myelin by oligodendrocytes is complex and requires precise temporal and spatial regulation of intracellular signals that control the various activities required for this crucial developmental process. While previous studies have shown that mTOR is important for oligodendrocyte differentiation and myelin formation, the effectors of mTOR signaling that drive differentiation and myelin formation are still not fully understood.

In earlier studies, we established that the impact of mTOR signaling in oligodendrocytes is different, depending on the CNS region that is examined (Bercury et al., 2014; Wahl et al., 2014), and indeed oligodendrocyte gene expression varies between brain and spinal cord precursor cells specifically (Khandker and Wood, 2022). In the earlier studies, we established that the loss of mTOR itself (Wahl et al., 2014) or of Raptor (mTORC1) (Bercury et al., 2014) results in reduced myelination in spinal cord, but not in corpus callosum. In those studies, loss of Rictor (mTORC2) had little impact in either region (Bercury et al., 2014). In our studies and in a comparable study from the Suter laboratory (Lebrun-Julien et al., 2014), Rictor was deleted from oligodendrocyte lineage cells using the CNP promoter. CNP is typically considered a late marker of oligodendrocyte development; for example, CNP RNA is barely detectable in OPCs by single-cell RNAseq (Marques et al., 2016). Thus, the earlier studies clearly showed that deletion of mTORC2 signaling from late differentiating/myelinating oligodendrocytes had relatively little impact on myelination throughout the CNS.

By contrast, in the current study, we establish that mTORC2 does indeed have a role in oligodendrocyte development and deleting mTORC2 early in OPC differentiation is detrimental. An earlier study by Grier et al. (2017) established that Rictor conditional deletion from all Olig2$^+$ cells resulted in reduced oligodendrocytes and myelination in cortex. The authors suggested that the reduction in oligodendrocyte number might result from an embryonic impact of Rictor loss in Olig2$^+$ cells, presumably from very early progenitors, and that it resulted in a delay in myelination that eventually recovered. The current studies confirm the results of Grier et al. (2017) on the impact of Rictor deletion but would not support the conclusion that this outcome results from an embryonic impact on oligodendrocyte cell number. Our studies delete Rictor only from PDGFRα-expressing cells, which would not be embryonic progenitor cells impacted in the earlier Olig2-based model. Rictor deletion from postnatal OPCs in corpus callosum resulted in reduced total oligodendrocytes, with a far greater impact on the number of maturing oligodendrocytes (Fig. 2). Furthermore, deletion of Rictor from OPCs resulted in permanent loss of Rictor and mTORC2 signaling and in long-term hypomyelination which extended into adulthood (Fig. 8).

More importantly, the current studies establish an unexpected regional impact of mTORC2 signaling on oligodendrocyte development. The regional impact of Raptor or mTOR loss from later stage oligodendrocytes established that the primary impact of mTOR or Raptor loss was in spinal cord, and there was little impact in corpus callosum during development (Bercury et al., 2014; Lebrun-Julien et al., 2014; Wahl et al., 2014). By contrast, in the Rictor cKO mice investigated here, differentiation and myelination in spinal cord were relatively spared, while loss of Rictor from OPCs specifically in the corpus callosum had a dramatic impact reducing myelination. Thus, the regional differences in mTORC2 requirement seen in this study are the exact opposite of those resulting from the loss of mTOR itself or of Raptor (Bercury et al., 2014; Lebrun-Julien et al., 2014; Wahl et al., 2014).

These differences did not result from an inability to delete Rictor or to impact the known function of mTORC2 to phosphorylate Akt at S473 in spinal cord OPCs, as spinal cord samples clearly had reduced Rictor and p-AktS473 (Figs. 1, 6). However, it may result from differences in endogenous PKCα or PKCβ$_{II}$ signaling, as we found that endogenous phosphorylation of PKCα/β$_{II}$ was not detected in the control spinal cord from P7 to P30 (Fig. 6B). Since endogenous phospho-PKCα/β$_{II}$ was present in control corpus callosum and it was significantly downregulated in Rictor cKO corpus callosum, this may be a major driver of mTORC2 signaling during OPC differentiation in corpus callosum, whereas mTORC2 signaling in spinal cord presumably does not involve PKCα/βII. PKC signaling pathways in oligodendrocytes have been implicated in OPC differentiation and vesicle trafficking (Uhm et al., 1998; Siskova et al., 2006; Baer et al., 2009), which clearly occur in spinal cord myelination, but oligodendrocytes of the spinal cord may use different signaling pathways for the same functions.

The importance of mTORC2 signaling particularly during OPC differentiation was highlighted by the complete loss of endogenous pAKT-S473 signaling in the corpus callosum of aged animals (Fig. 8). mTOR has an important role in myelin maintenance of the corpus callosum (Khandker and Wood, 2022), and our results would indicate that this maintenance role is likely mTORC1 specific and that mTORC2 may be less important after the initial differentiation stage. Furthermore, the almost complete

---

matter (open bars) or gray matter (gray bars). Paired t test. Statistical information is given in a table below each corresponding graph and includes n, SEM, mean of corpus callosum (white matter), p value, and degrees of freedom (df). **E**, Corpus callosum widths were measured using F-actin/G-actin-stained images at the approximate midline of control compared with Rictor cKO mice in P14 and P30. **F–K**, Quantification of actin regulators in corpus callosum of CNT and cKO mice. **F**, Western blot: Gelsolin in corpus callosum; CNT and cKO at P7, P14, P30 and in aged mice. **G**, Western blot: Gelsolin in the spinal cord at ages P7, P14, and P30. **H**, Western blot: Profilin1 in corpus callosum at ages P7, P14, and P30. **I**, Western blot: Profilin1 in the spinal cord at ages P7, P14, and P30. **J**, Western blot: Profilin2 in corpus callosum at ages P7, P14, and P30. **K**, Western blot: Profilin2 in spinal cord at ages P7, P17, and P30. Unpaired t test with Welch's correction. Statistical information is given in a table below each corresponding graph and includes age, n (written as control and cKO), p value, SEM for control, mean of cKO, SEM for cKO, and degrees of freedom (df).
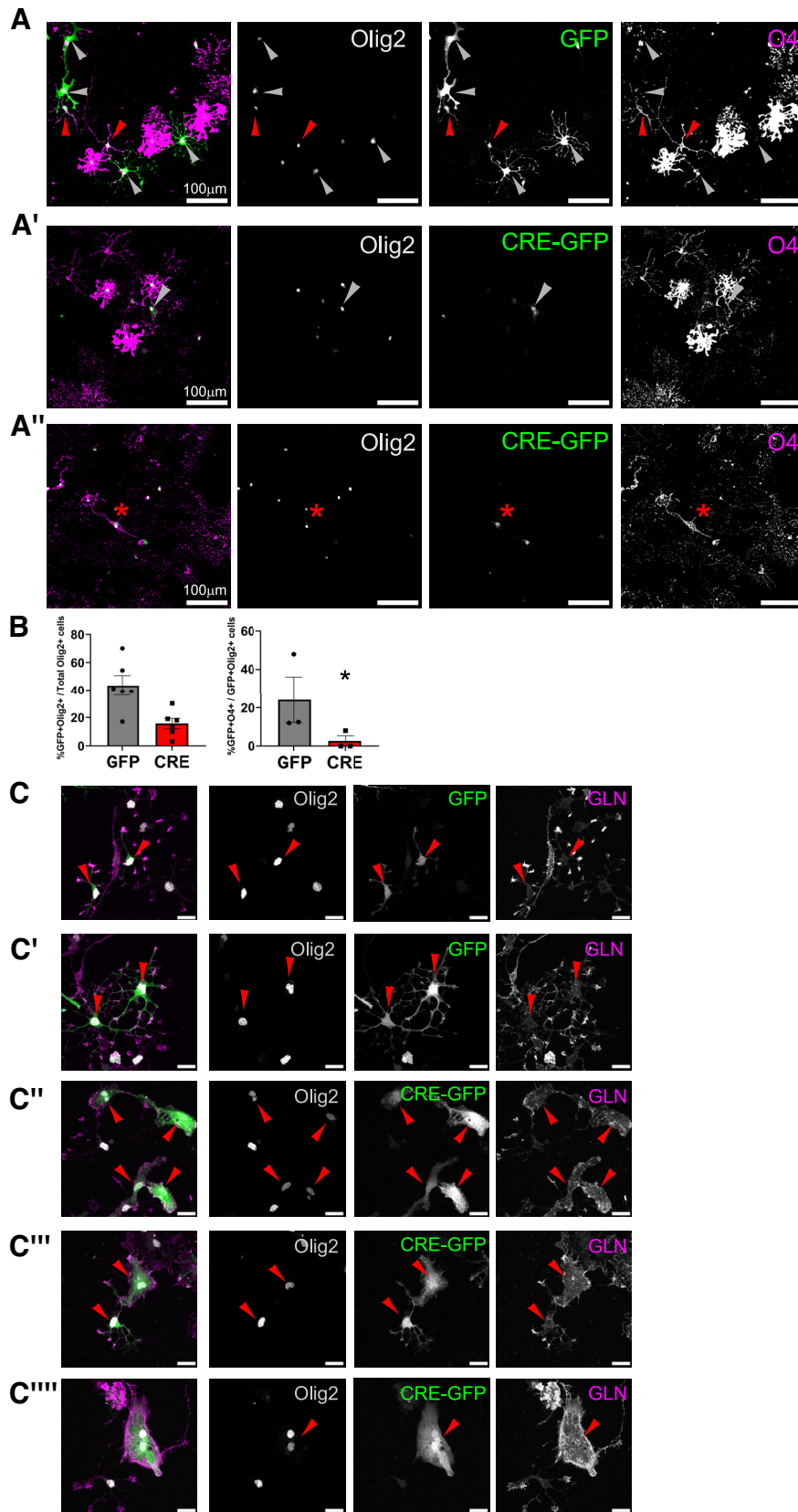
Figure 10. Cre expression in Rictor^{fl/fl} OPCs *in vitro* resulted in impaired differentiation. *In vitro* treatment of Rictor^{fl/fl} mouse OPCs with Cre resulted in few differentiated oligodendrocyte lineage cells. **A**, Mouse OPCs isolated from Rictor^{fl/fl} animals were treated with either adenovirus GFP or adenovirus Cre GFP. Fixed cells were stained for Olig2 and O4 antibody. **A**, GFP-transduced cells. **A′–A′′**, GFP/Cre-transduced cells. Left to right, Merged image (Olig2 [gray], GFP [green], and O4 [magenta]), Olig2, GFP, and O4. Red arrowheads indicate cells positive for Olig2, GFP, and O4 (differentiating cells). Gray arrowheads indicate cells positive for Olig2 and GFP, not O4 (OPCs). Red asterisk highlights the only O4[+] cell present in GFP/Cre-transduced cells. Scale bar, 100 μm. **B**, Quantification of transduction efficiency for virus-treated oligodendrocytes and quantification of dual-labeled GFP and O4[+] oligodendrocytes. %GFP[+]Olig2^{+}/total Olig2^{+} cells (GFP mean = 43%, n = 6 experiments, SEM ± 7.231; Cre mean = 16%, n = 6 experiments, SEM ± 3.730; nonparametric Mann–Whitney test p = 0.0130) %GFP[+]O4[+]/GFP[+]Olig2^{+} cells (GFP

inhibition of OPC differentiation into $O4^+$ cells on Rictor loss *in vitro* (Fig. 10) further highlighted the importance of mTORC2 for initial oligodendrocyte differentiation in brain.

The current studies focus extensively on the signaling impact of the loss of mTORC2 in OPCs. Importantly, the impact of Rictor loss on oligodendrocyte differentiation during early brain development in corpus callosum did not alter mTORC1 signaling (Fig. 4). However, by P30, the loss of mTORC2 in later stages of corpus callosum myelination did alter mTORC1 signaling, reducing S6RP phosphorylation. Interestingly, neither pAkt-T308, the Akt phosphorylation substrate of phosphoinositide-dependent kinase 1 driving mTORC1 signaling, nor phosphorylation of mTOR itself at S2448, which is the S6RP negative feedback regulator of mTORC1 signaling (Figueiredo et al., 2017), was affected at late stages of development. Likely, the overall impact on myelination resulting from loss of mTORC2 signaling reduced oligodendrocyte differentiation in corpus callosum in general.

One of our recent studies (Musah et al., 2020) showed that the inhibition of mTOR signaling in cultured OPCs or loss of mTOR in oligodendrocytes *in vivo* results in a decrease in Profilin2, a member of the profilin family that is quite abundant in the brain. However, deleting mTORC2 signaling in OPCs in the current study resulted in no change in Profilin2 in corpus callosum. Thus, mTORC1 is likely responsible for the loss of Profilin2 in mTOR cKO mice, where it has a greater impact on spinal cord myelination. On the other hand, loss of mTORC2 did result in small reduction of the more ubiquitous Profilin1 at P14, which may indicate some direct regulation of Profilin1 expression by mTORC2. However, Profilin1 was reduced in both corpus callosum and spinal cord at P14, suggesting that it does not drive the differential impact of Rictor loss from OPCs in corpus callosum and spinal cord. Our prior study (Musah et al., 2020) also indicated that loss of mTOR regulates a variety of cytoskeletal processes in differentiating oligodendrocytes in spinal cord. The lack of a major effect of Rictor loss on oligodendrocyte differentiation in the spinal cord suggests that much of this occurs independently of mTORC2, likely through mTORC1, whereas the corpus callosum relies more on mTORC2 for oligodendrocyte differentiation. This is also supported by our prior findings on the Raptor cKO mice (i.e., reduced mTORC1 signaling) where oligodendrocyte differentiation was compromised specifically in spinal cord (Bercury et al., 2014).

The loss of mTORC2 signaling resulted in a dramatic loss of gelsolin in corpus callosum from P14 (i.e., the time of active OPC differentiation and myelination). No loss of gelsolin was seen in spinal cord, which could be a key difference in the impact of mTORC2 deletion from OPCs. Gelsolin is a Ca^{2+}- and polyphosphoinositide 4,5-bisphosphate-regulated actin binding protein whose major activity is in filamentous actin severing, which it does with close to 100% efficiency (Selden et al., 1998). Gelsolin is involved in oligodendrocyte differentiation and myelination. It is highly expressed in the oligodendrocyte lineage, with greatest expression in actively myelinating cells, but with

significant expression in newly formed oligodendrocytes (Zhang et al., 2014). It is proposed to be sequestered at the plasma membrane before the production of MBP, which then displaces it at the membrane, releasing this actin-severing protein to drive actin disassembly (Zuchero et al., 2015). In its absence, the actin polymerization/depolymerization cycle would be nonfunctional, reducing the ability to generate compact myelin. Presumably, this cycle must be differentially regulated in corpus callosum and spinal cord oligodendrocytes.

In the corpus callosum of Rictor cKOs, there were fewer myelinated axons; but among the myelinated axons in corpus callosum, g-ratios in Rictor cKO and controls were quite similar. This indicates that, although fewer OPCs in the Rictor cKO mice were able to differentiate, those that did progress to myelination ensheathed axons with the appropriate amount of myelin. A larger proportion of myelinated axons in the Rictor cKO had reduced diameters compared with controls. This suggests that the smaller axons in the Rictor cKO were more likely to be myelinated. By contrast, in the Grier et al. (2017) study, the average myelinated axon diameter in the cKO corpus callosum was thicker than control, suggesting that deletion of Rictor at different stages of OPC development may bias axon selection. These studies suggest that mTORC2 signaling appears important for the initial differentiation of OPCs and premyelinating cells; but once cells differentiated beyond the earliest stages of myelination, other regulators drive the late stages of myelination. This may explain the relatively minor impact of mTORC2 loss in CNP-Cre mice, where the deletion would have been at the later stages of oligodendrocyte differentiation. This may also explain the recovery seen in the Olig2-Cre-deleted mice as they age (Grier et al., 2017). Thus, it may be in that model, if the Olig2 promoter is less active in older animals, some cells might escape loss of mTORC2 signaling; and once past the differentiation stage, they may be able to produce increasing amounts of myelin.

Further examination of the role of mTORC2 in oligodendrocyte development is necessary to elucidate the full impact of this kinase. We still do not know the direct targets of mTORC2 in oligodendrocytes. It is intriguing to speculate about the relative importance of mTORC2 signaling at different stages of oligodendrocyte differentiation. Clearly, both this study and Grier et al. (2017) demonstrate that deletion of Rictor is detrimental to OPC differentiation in corpus callosum, while our earlier study with CNP-Cre driven deletion of Rictor (Bercury et al., 2014) showed normal oligodendrocyte differentiation but early loss of myelin RNAs from corpus callosum with some recovery by P29, and essentially normal myelin thickness by 2 months of age. Thus, loss of mTORC2 signaling after early OPC differentiation impacted gene expression, but there was sufficient recovery that normal myelin was produced. Both our previous study (Bercury et al., 2014) and that of Lebrun-Julien et al. (2014) showed little impact in spinal cord, but the current study suggests that no impact would have been expected regardless of the timing of Rictor deletion from spinal cord oligodendrocytes. Building on the findings here, studies investigating the impact of Rictor/mTORC2 signaling with respect to cytoskeleton reorganization in the differentiating oligodendrocyte are underway to determine how mTORC2 signaling regulates OPC differentiation.

The current studies identify regional differences in mTORC2 loss in corpus callosum relative to spinal cord. The unanswered question is what causes this regional difference. Our data on the impact of mTOR, likely mTORC1, also establish regional differences (Khandker and Wood, 2022), and an extensive analysis of

gene expression differences suggests that local environmental cues may be important. The cholesterol biosynthesis and uptake pathways are differentially regulated in OPCs from the two regions, and cholesterol availability in the two regions may be important. Conversely, embryonic origin may be relevant, as cortical and spinal cord OPCs are generated from different precursor populations. Cortical cells arise from the subventricular zone (Pringle and Richardson, 1993; Tekki-Kessaris et al., 2001) and spinal cord cells from the ventral ventricular zone of the spinal cord (Warf et al., 1991; Pringle and Richardson, 1993; Ono et al., 1995; Timsit et al., 1995). Both precursor populations are exposed to unique local signals (Orentas and Miller, 1996; Mehler, 2002; Shimogori et al., 2004), which may fundamentally alter their development. Further investigation will provide insight into the underlying mechanisms driving the regional regulation of oligodendrocyte differentiation and myelination.

References

Adams KL, Dahl KD, Gallo V, Macklin WB (2021) Intrinsic and extrinsic regulators of oligodendrocyte progenitor proliferation and differentiation. Semin Cell Dev Biol 116:16–24.

Baer AS, Syed YA, Kang SU, Mitteregger D, Vig R, Ffrench-Constant C, Franklin RJ, Altmann F, Lubec G, Kotter MR (2009) Myelin-mediated inhibition of oligodendrocyte precursor differentiation can be overcome by pharmacological modulation of Fyn-RhoA and protein kinase C signalling. Brain 132:465–481.

Bercury KK, Dai J, Sachs HH, Ahrendsen JT, Wood TL, Macklin WB (2014) Conditional ablation of raptor or Rictor has differential impact on oligodendrocyte differentiation and CNS myelination. J Neurosci 34:4466–4480.

Bustin SA, Benes V, Garson JA, Hellemans J, Huggett J, Kubista M, Mueller R, Nolan T, Pfaffl MW, Shipley GL, Vandesompele J, Wittwer CT (2009) The MIQE guidelines: minimum information for publication of quantitative real-time PCR experiments. Clin Chem 55:611–622.

Carpenter AE, Jones TR, Lamprecht MR, Clarke C, Kang IH, Friman O, Guertin DA, Chang JH, Lindquist RA, Moffat J, Golland P, Sabatini DM (2006) CellProfiler: image analysis software for identifying and quantifying cell phenotypes. Genome Biol 7:R100.

Copp J, Manning G, Hunter T (2009) TORC-specific phosphorylation of mammalian target of rapamycin (mTOR): phospho-Ser2481 is a marker for intact mTOR signaling complex 2. Cancer Res 69:1821–1827.

Figueiredo VC, Markworth JF, Cameron-Smith D (2017) Considerations on mTOR regulation at serine 2448: implications for muscle metabolism studies. Cell Mol Life Sci 74:2537–2545.

Flores AI, Narayanan SP, Morse EN, Shick HE, Yin X, Kidd G, Avila RL, Kirschner DA, Macklin WB (2008) Constitutively active Akt induces enhanced myelination in the CNS. J Neurosci 28:7174–7183.

Franklin KB, Paxinos G (2008) Mouse brain in stereotaxic coordinates. New York, NY: Academic Press.

Goldman JE (1992) Regulation of oligodendrocyte differentiation. Trends Neurosci 15:359–362.

Grier MD, West KL, Kelm ND, Fu C, Does MD, Parker B, McBrier E, Lagrange AH, Ess KC, Carson RP (2017) Loss of mTORC2 signaling in oligodendrocyte precursor cells delays myelination. PLoS One 12: e0188417.

Khandker L, Wood TL (2022) Live-cell metabolic analysis of oligodendroglia isolated from postnatal mouse brain and spinal cord. STAR Protoc 3:101655.

Lebrun-Julien F, Bachmann L, Norrmen C, Trotzmuller M, Kofeler H, Ruegg MA, Hall MN, Suter U (2014) Balanced mTORC1 activity in oligodendrocytes is required for accurate CNS myelination. J Neurosci 34:8432–8448.

Marques S, et al. (2016) Oligodendrocyte heterogeneity in the mouse juvenile and adult central nervous system. Science 352:1326–1329.

Mathews ES, Appel B (2016) Cholesterol biosynthesis supports myelin gene expression and axon ensheathment through modulation of P13K/Akt/mTor signaling. J Neurosci 36:7628–7639.

Mehler MF (2002) Mechanisms regulating lineage diversity during mammalian cerebral cortical neurogenesis and gliogenesis. Results Probl Cell Differ 39:27–52.

Musah AS, Brown TL, Jeffries MA, Shang Q, Hashimoto H, Evangelou AV, Kowalski A, Batish M, Macklin WB, Wood TL (2020) Mechanistic target of rapamycin regulates the oligodendrocyte cytoskeleton during myelination. J Neurosci 40:2993–3007.

Narayanan SP, Flores AI, Wang F, Macklin WB (2009) Akt signals through the mammalian target of rapamycin pathway to regulate CNS myelination. J Neurosci 29:6860–6870.

Nawaz S, Sanchez P, Schmitt S, Snaidero N, Mitkovski M, Velte C, Bruckner BR, Alexopoulos I, Czopka T, Jung SY, Rhee JS, Janshoff A, Witke W, Schaap IA, Lyons DA, Simons M (2015) Actin filament turnover drives leading edge growth during myelin sheath formation in the central nervous system. Dev Cell 34:139–151.

Oh WJ, Jacinto E (2011) mTOR complex 2 signaling and functions. Cell Cycle 10:2305–2316.

Ono K, Bansal R, Payne J, Rutishauser U, Miller RH (1995) Early development and dispersal of oligodendrocyte precursors in the embryonic chick spinal cord. Development 121:1743–1754.

Orentas DM, Miller RH (1996) The origin of spinal cord oligodendrocytes is dependent on local influences from the notochord. Dev Biol 177:43–53.

Pringle NP, Mudhar HS, Collarini EJ, Richardson WD (1992) PDGF receptors in the rat CNS: during late neurogenesis, PDGF alpha-receptor expression appears to be restricted to glial cells of the oligodendrocyte lineage. Development 115:535–551.

Pringle NP, Richardson WD (1993) A singularity of PDGF alpha-receptor expression in the dorsoventral axis of the neural tube may define the origin of the oligodendrocyte lineage. Development 117:525–533.

Roesch K, Jadhav AP, Trimarchi JM, Stadler MB, Roska B, Sun BB, Cepko CL (2008) The transcriptome of retinal Muller glial cells. J Comp Neurol 509:225–238.

Saxton RA, Sabatini DM (2017) mTOR signaling in growth, metabolism, and disease. Cell 169:361–371.

Schindelin J, Arganda-Carreras I, Frise E, Kaynig V, Longair M, Pietzsch T, Preibisch S, Rueden C, Saalfeld S, Schmid B, Tinevez JY, White DJ, Hartenstein V, Eliceiri K, Tomancak P, Cardona A (2012) Fiji: an open-source platform for biological-image analysis. Nat Methods 9:676–682.

Selden LA, Kinosian HJ, Newman J, Lincoln B, Hurwitz C, Gershman LC, Estes JE (1998) Severing of F-actin by the amino-terminal half of gelsolin suggests internal cooperativity in gelsolin. Biophys J 75:3092–3100.

Shimogori T, Banuchi V, Ng HY, Strauss JB, Grove EA (2004) Embryonic signaling centers expressing BMP, WNT and FGF proteins interact to pattern the cerebral cortex. Development 131:5639–5647.

Shiota C, Woo JT, Lindner J, Shelton KD, Magnuson MA (2006) Multiallelic disruption of the Rictor gene in mice reveals that mTOR complex 2 is essential for fetal growth and viability. Dev Cell 11:583–589.

Siskova Z, Baron W, de Vries H, Hoekstra D (2006) Fibronectin impedes 'myelin' sheet-directed flow in oligodendrocytes: a role for a beta 1 integrin-mediated PKC signaling pathway in vesicular trafficking. Mol Cell Neurosci 33:150–159.

Tekki-Kessaris N, Woodruff R, Hall AC, Gaffield W, Kimura S, Stiles CD, Rowitch DH, Richardson WD (2001) Hedgehog-dependent oligodendrocyte lineage specification in the telencephalon. Development 128:2545–2554.

Timsit S, Martinez S, Allinquant B, Peyron F, Puelles L, Zalc B (1995) Oligodendrocytes originate in a restricted zone of the embryonic ventral neural tube defined by DM-20 mRNA expression. J Neurosci 15:1012–1024.

Tyler WA, Gangoli N, Gokina P, Kim HA, Covey M, Levison SW, Wood TL (2009) Activation of the mammalian target of rapamycin (mTOR) is essential for oligodendrocyte differentiation. J Neurosci 29:6367–6378.

Uhm JH, Dooley NP, Oh LY, Yong VW (1998) Oligodendrocytes utilize a matrix metalloproteinase, MMP-9, to extend processes along an astrocyte extracellular matrix. Glia 22:53–63.

Verden D, Macklin WB (2016) Neuroprotection by central nervous system remyelination: Molecular, cellular and functional considerations. J Neurosci Res 94:1411–1420.

Wahl SE, McLane LE, Bercury KK, Macklin WB, Wood TL (2014) Mammalian target of rapamycin promotes oligodendrocyte differentiation, initiation and extent of CNS myelination. J Neurosci 34:4453–4465.

Warf BC, Fok-Seang J, Miller RH (1991) Evidence for the ventral origin of oligodendrocyte precursors in the rat spinal cord. J Neurosci 11:2477–2488.

Wood TL, Bercury KK, Cifelli SE, Mursch LE, Min J, Dai J, Macklin WB (2013) mTOR: a link from the extracellular milieu to transcriptional regulation of oligodendrocyte development. ASN Neuro 5:e00108.

Zaimi A, Wabartha M, Herman V, Antonsanti PL, Perone CS, Cohen-Adad J (2018) AxonDeepSeg: automatic axon and myelin segmentation from microscopy data using convolutional neural networks. Sci Rep 8:3816.

Zhang Y, Chen K, Sloan SA, Bennett ML, Scholze AR, O'Keeffe S, Phatnani HP, Guarnieri P, Caneda C, Ruderisch N, Deng S,

Liddelow SA, Zhang C, Daneman R, Maniatis T, Barres BA, Wu JQ (2014) An RNA-sequencing transcriptome and splicing database of glia, neurons, and vascular cells of the cerebral cortex. J Neurosci 34:11929–11947.

Zhou Q, Wang S, Anderson DJ (2000) Identification of a novel family of oligodendrocyte lineage-specific basic helix-loop-helix transcription factors. Neuron 25:331–343.

Zuchero JB, Fu MM, Sloan SA, Ibrahim A, Olson A, Zaremba A, Dugas JC, Wienbar S, Caprariello AV, Kantor C, Leonoudakis D, Lariosa-Willingham K, Kronenberg G, Gertz K, Soderling SH, Miller RH, Barres BA (2015) CNS myelin wrapping is driven by actin disassembly. Dev Cell 34:152–167.